The Astronomical Journal, 135:209–231, 2008 January
doi:10.1088/0004-6256/135/1/209

ROTATIONAL AND RADIAL VELOCITIES FOR A SAMPLE OF 761 HIPPARCOS GIANTS AND THE ROLE OF BINARITY*

Alessandro Massarotti[1,2], David W. Latham[1], Robert P. Stefanik[1], and Jeffrey Fogel[3,4]
[1] Harvard-Smithsonian Center for Astrophysics, 60 Garden Street, Cambridge, MA 02138, USA
[2] Department of Physics and Astronomy, Stonehill College, 320 Washington Street, Easton, MA 02357, USA; amassaro@cfa.harvard.edu
[3] Department of Astronomy, Harvard University, 60 Garden Street, Cambridge, MA 02138, USA
[4] Department of Astronomy, University of Michigan, 500 Church Street, Ann Arbor, MI 48109-1042, USA; fogel@umich.edu
Received 2007 July 31; accepted 2007 September 10; published 2007 December 7

ABSTRACT

We present rotational and radial velocities for a sample of 761 giants selected from the Hipparcos Catalogue to lie within 100 pc of the Sun. Our original goal was to examine stellar rotation in field giants using spectroscopic line broadening to look for evidence of excess rotation that could be attributed to planets that were engulfed as the parent stars expanded. Thus we were obliged to investigate other sources of line broadening, including tidal coupling in close binaries and macroturbulence. For all the binaries in our sample with periods shorter than 20 days the orbits have been circularized, while about half the orbits with periods in the range 20–100 days still show significant eccentricity. All our primaries in orbits shorter than 30 days show line broadening consistent with synchronized rotation, while about half the primaries with periods in the range 30–120 days are synchronized. To study the dependence of rotation on stellar evolution when tidal effects are not important, we used a subsample of single stars and members in wide binaries. We found evidence to suggest that the first dredge-up may play a role in speeding up the rotation of the observable outer layers of giants and that the rotational velocity of horizontal branch stars is larger by a few km s^{-1} than that of first-ascent giants with similar mass, effective temperature, and radius. Finally, we found three giants that rotate more rapidly than expected. We conjecture that they acquired their excess angular momentum by ingesting planets.

Key words: stars: AGB and post-AGB – stars: evolution – stars: rotation – binaries: spectroscopic – planetary systems – techniques: spectroscopic

Online-only material: machine-readable tables

1. INTRODUCTION

The discovery of a population of giant planets around solar-type stars in orbits smaller than 1 AU lends some urgency to the question of what happens when a main-sequence star evolves into a giant large enough to engulf such a planet. How much orbital angular momentum from the planet gets converted into excess rotation of the outer layers of the evolving star? Is the effect observable, and how long does it last?

On the theoretical side, the ingestion of giant planets and brown dwarfs by evolving giant stars was studied by Livio (1982), followed by Livio & Soker (1984), Soker et al. (1984), Siess & Livio (1999a, 1999b), and Sandquist et al. (1998, 2002). Various scenarios for the interaction between the companion and the evolving star have been considered. According to Livio & Soker (1984) and Soker et al. (1984), when a giant engulfs a companion smaller than about 20 Jupiter masses, that should lead to its ingestion by the star.

On the observational side, Carney et al. (2003) measured spectral line broadening in a sample of 91 metal-poor red giants and found evidence of excess broadening in a few of the most swollen stars near the tip of the giant branch, and also in some of the post-tip stars on the horizontal branch. They suggested that excess rotation due to ingestion of planets near the tip might be the explanation for the observed excess broadening.

Motivated by this result, that some metal-poor red giants appear to show excess rotation, we undertook a similar survey of a much larger sample of 761 evolved stars drawn from the Hipparcos Catalogue (ESA 1997). Would a sample of solar-metallicity red giants also show evidence for ingested planets? Could the relative frequency of excess rotation between the two samples be used to evaluate the relative roles of core accretion versus disk instability in the formation of giant planets? How about the possibility that the role of planetary migration might depend on metallicity?

As often happens in scientific research, the answers to our naive questions became more elusive as we learned more about the problem. Rotation in an evolving star is not simply the result of conservation of angular momentum applied to an object whose moment of inertia evolves. For single stars, the onset of a stellar wind and magnetic dynamo can provide a strong braking mechanism that carries away rotational angular momentum if the stellar wind is forced to corotate with the star as the wind flows outward. This mechanism is effective at reducing rotation when corotation extends out to several stellar radii. It is thought to be responsible for the dramatic transition from rapid to slow rotation near spectral type F8 on the main sequence (e.g., see Barnes 2000), corresponding to about 1.3 $M_\odot$. Lower-mass stars inherit almost no rotation, at least of their observable outer layers, as they evolve away from the main sequence, while higher mass stars inherit projected rotational velocities $V_{\rm rot} \sin i$ that often exceed 100 km s^{-1} with a Maxwell–Boltzmann distribution (Gray 1989). As these stars cross the so-called granulation boundary on the Hertzsprung–Russell (H–R) diagram (Strassmeier et al. 1998), they develop a convective envelope that gradually deepens, eventually leading to a magnetic dynamo and stellar wind, as evidenced by active

* Some of the results presented here used observations made with the Multiple Mirror Telescope, a joint facility of the Smithsonian Institution and the University of Arizona.

coronas. The resulting strong rotational braking is manifested observationally as a sharp transition to slow rotation on the giant branch at spectral type G0 to G3 (Strassmeier et al. 1998; Gray 1989; De Medeiros et al. 1996, 2000, 2003; De Medeiros & Mayor 1999). This strong braking appears to act only until the equatorial rotational velocity falls close to the macroturbulent velocity (Gray 1989). After that stars seem to lose angular momentum slowly (if at all), as they evolve toward the tip of the giant branch during the advanced stages of the hydrogen shell burning phase. Indeed, it has been suggested that the outer layers may actually be spun up if the stellar core is rotating rapidly and a coupling to the observable surface can be established (e.g., see Demarque et al. 2001).

In the case of close binaries, tidal torques can be much stronger than the rotational braking due to magnetic coupling with a stellar wind, and the orbital angular momentum can dominate and control the stellar rotation. Tidal mechanisms tend to align the stellar rotation axes with the orbital axis, to synchronize the rotational periods with the orbital period, and to circularize the orbit, normally with the sequence of events in this order (e.g., see Zahn 1989). Studies of binaries with a giant component include those of Mermilliod & Mayor (1992) and De Medeiros et al. (2002, 2004). Observationally, the transition from eccentric to circular orbits occurs at a period of roughly 150 days for giant binaries in open clusters (e.g., see Mermilliod & Mayor 1992).

Thus, to allow the identification of isolated giants with excess rotation, it was first necessary to identify all the stars where the rotation could be attributed to tidal coupling in a binary. For many of the binaries in our sample, spectroscopic orbits were already available in the literature (e.g., see Pourbaix et al. 2004). For giants that were not known to be binaries, our strategy was to use an initial pair of observations to determine the line broadening. If there was an indication of excess broadening, we then accumulated additional observations over a time span of 1 or 2 years with the goal of identifying all the giants with stellar companions in orbits with periods shorter than a few hundred days, to see if the excess broadening could be attributed to tidal mechanisms. Thus, in 47 cases we accumulated enough observations to allow for orbital solutions using just our own radial velocities, including nine single-lined and four double-lined binaries with no previously published orbits. In addition, we obtained new velocities for 23 binaries with published orbits, so we could update the solutions with modern observations. We also revised four previously published solutions by analyzing the old velocities with modern software. We then used all the stars where tidal mechanisms are negligible to explore how stellar rotation depends on evolutionary stage for giants.

In the end, we were left with only three giants where there is excess rotation that cannot be explained easily and therefore may be due to the ingestion of giant planets.

2. SAMPLE SELECTION

We utilized the Hipparcos Catalogue (ESA 1997) to select a sample of giants with distances within 100 pc. Since the typical accuracy for a Hipparcos parallax is 1 mas, the distances to our targets are accurate to about 10% or better, and the absolute magnitudes to 0.2 mag or better. We limited the sample to the declination range from -20° to $+60^\circ$, because we wanted to use the CfA Digital Speedometer (Latham 1992) on the 1.5 m Wyeth Reflector at the Oak Ridge Observatory located in the town of Harvard, MA, where the northern limit is set by the fork mount, and the southern limit is set by oak trees. For stars with $B-V<1.3$ mag we selected all the giants more than nominally 2.5 mag above the main sequence (absolute V magnitude $M_V<1.44+5.15(B-V)$), for stars with $1.3 \leqslant (B-V) \leqslant 2.5$ mag we selected all the giants more than 6 mag above the main sequence ($M_V<7.44+5.15(B-V)$), and for stars redder than $(B-V)=2.5$ mag we selected only the giants brighter than apparent magnitude $V=8$. The 761 giants selected in this way are plotted with the symbol $\times$ on the color versus absolute magnitude diagram in Figure 1, together with the dividing lines defined above. In several cases, the light from these targets is a composite of two or more individual stars, including a giant. Stars meeting the distance and declination criteria but too faint to pass the absolute magnitude selection are plotted as small dots.

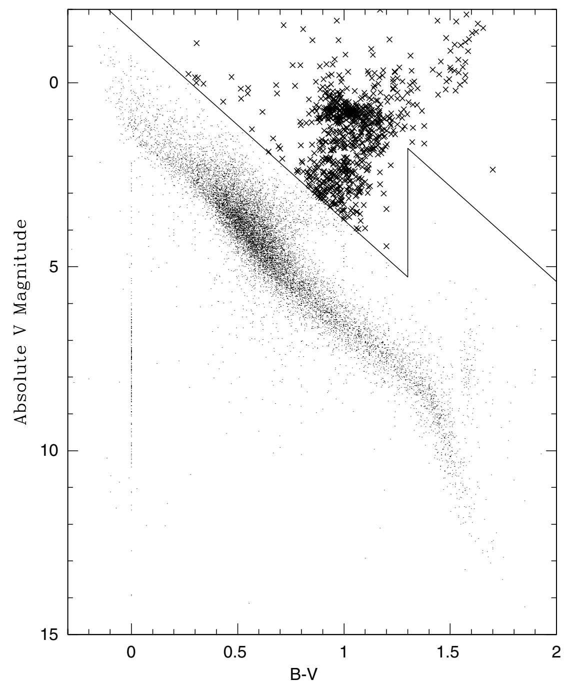

Figure 1. Color–magnitude diagram for Hipparcos stars within 100 pc. The giants in our sample are plotted with the symbol $\times$.

Because our sample of giants was selected from the Hipparcos Catalogue to lie within 100 pc, the stars are all quite bright, as shown in Figure 2. More than half the stars are sixth magnitude or brighter, and thus are easy to observe even under mediocre conditions. Indeed, for the brightest stars in the sample we found it necessary to reduce the light entering the spectrograph slit by means of a neutral density filter (or clouds), to avoid pulse pile-up in the photon-counting intensified Reticon detector. Table 1 is a list of our program stars by Hipparcos number, together with the HD, HR, Flamsteed, and Bayer aliases reported by Vizier (Ochsenbein et al. 2000) and the J2000 positions from the 2MASS Catalog (Skrutskie et al. 2006).

3. ROTATIONAL AND RADIAL VELOCITIES

We measured new rotational and radial velocities for all the stars in our sample using the CfA Digital Speedometers (Latham 1992), primarily with the 1.5 m Wyeth Reflector at the Oak Ridge Observatory, but also with nearly identical instruments on the 1.5 m Tillinghast Reflector and on the MMT, both located at the Whipple Observatory atop Mount Hopkins, AZ. These instruments record a single echelle order covering 45 Å centered

Table 1
Program Stars, Aliases, and Positions

Star	HD	HR	Name	2MASS RA	2MASS Dec
HIP000343 . . .	225 197	9101	. . .	00 04 19.79	−16 31 44.3
HIP000443 . . .	28	3	33 Psc	00 05 20.13	−05 42 27.5
HIP000626 . . .	290	. . .	. . .	00 07 37.91	+40 08 52.2
HIP000729 . . .	448	22	87 Peg	00 09 02.43	+18 12 43.2
HIP000840 . . .	587	29	. . .	00 10 18.87	−05 14 54.9

(This table is presented in its entirety in a machine-readable form in the online journal. A portion is shown here for guidance regarding its form and content)

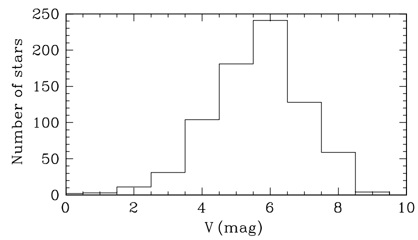

Figure 2. Number of program stars as a function of visual magnitude V.

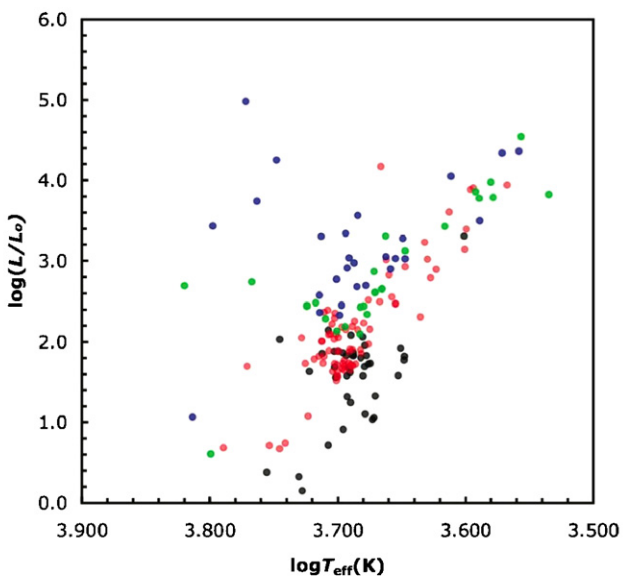

Figure 3. Macroturbulence from Gray and coworkers as a function of $\log(L/L_\odot)$ and $\log T_{\rm eff}$. The color coding is black for $2 \leqslant \zeta_{\rm RT} < 5$, red for $5 \leqslant \zeta_{\rm RT} < 7$, green for $7 \leqslant \zeta_{\rm RT} < 9$, and blue for $\zeta_{\rm RT} \geqslant 9$, all in km s^{-1}.

at 5187 Å using photon-counting intensified Reticon detectors. The spectral resolution of all three CfA Digital Speedometers is nominally 8.5 km s^{-1}, and the typical signal-to-noise ratio (SNR) per resolution element ranged from 15 to 50, depending primarily on the amount of line broadening (rapidly rotating stars were exposed for longer on purpose).

The rotational and radial velocities were determined by cross correlation of the observed spectra against templates drawn from a library of synthetic spectra calculated by Jon Morse for a grid of Kurucz (1992) stellar atmospheres. The library grid has a spacing of 250 K in effective temperature, $T_{\rm eff}$, 0.5 in log surface gravity, $\log g$, and 0.5 in log metallicity relative to the sun, [Fe/H]. For each star, we selected the template having these three parameters closest to the values that we extracted from information in the literature, as described in the following section. We then ran correlations for the full grid of rotational

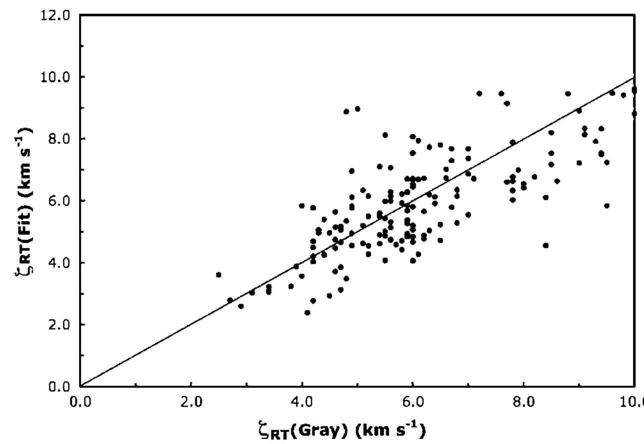

Figure 4. Gray's measured values of $\zeta_{\rm RT}$ compared to fitted values from Equation (1).

values, $V_{\rm rot} = 0, 1, 2, 4, 6, 8, 10, 12, 16, 20, 25, 30, 35, 40, 50, 60, 70, 80, 90, 100, 120, 140$ km s^{-1} and calculated the mean value of the peak correlation coefficient at each rotation. Next, we used a quadratic interpolation for the three templates centered on the rotation with the highest correlation coefficient to derive the final line broadening for that choice of template parameters, ($T_{\rm eff}$, $\log g$, [Fe/H]). Finally, we repeated the process for templates 250 K hotter and 250 K cooler in $T_{\rm eff}$, and interpolated quadratically to get the final rotation at the $T_{\rm eff}$ derived from photometry.

The final radial velocities for each exposure of a star were calculated using the template rotation that gave the highest correlation coefficient averaged over all the exposures for that star.

The procedures used here to determine rotational velocities are similar to the procedures used by Carney et al. (2003), except that here we used our standard library of synthetic spectra appropriate for solar-metallicity giants, rather than the library with enhanced α-element abundances appropriate for very metal-poor giants. A more important difference is our treatment of macroturbulence in this paper. Our stellar models and synthetic spectra were all calculated assuming a microturbulence of 2 km s^{-1}, which is approximately correct for giants (McWilliam 1990), and a value for macroturbulence of $\zeta_{\rm RT} = 1.5$ km s^{-1}, which is generally too small for giants. In reality, macroturbulence ranges from about 2 km s^{-1} for subgiants up to as much as 16 km s^{-1} for supergiants (e.g., see Figure 4). Thus the rotation of the synthetic template spectrum that gives the best match to an observed spectrum is really a proxy for line broadening, and must be corrected for the larger value of macroturbulence appropriate for the star being observed in order to give an estimate of the actual projected rotational velocity, $V_{\rm rot} \sin i$, as discussed below.

Table 2
Color Indexes

Star	$B-V$	B_T-V_T	$V-J$	$V-H$	$V-K$	$C(45-48)$	$C(42-45)$
HIP000343 ...	1.099	1.295	...	...	...	1.213	0.932
HIP000443 ...	1.040	1.220	...	...	...	1.190	0.912
HIP000626 ...	0.947	1.102	1.707	2.165	2.245	...	...
HIP000729 ...	1.045	1.227	...	...	...	...	...
HIP000840 ...	0.978	1.142	...	...	...	1.163	0.870

(This table is presented in its entirety in a machine-readable form in the online journal. A portion is shown here for guidance regarding its form and content)

Table 3
Physical Parameters of the Program Stars

Star	d	σ_d	T_{eff}	σ_T	$\log(L/L_\odot)$	$R/R_\odot$	$\log g$	Refs	[Fe/H]	Refs
HIP000343 ...	89	7	4613	5	1.65	10	2.5	1	...	...
HIP000443 ...	39	2	4699	9	1.39	7	2.8	1	−0.31	5
HIP000626 ...	99	7	4842	24	1.30	6	3.0	1	...	...
HIP000729 ...	90	6	4710	0	1.72	11	2.7	1	−0.01	5
HIP000840 ...	55	3	4819	10	1.15	5	2.9	1	−0.24	5

Notes. Entries for T_{eff}, σ_T, $\log(L/L_\odot)$, and $R/R_\odot$ were left blank for all double-lined binaries and for single-lined binaries with a known composite spectrum. The physical parameters for the giants in these binaries can be found in Tables 14 and 15.
References. (1) Allende Prieto & Lambert (1999), (2) McWilliam (1990), (3) our values, (4) Valdez et al. (2004), and (5) McWilliam (1990).
(This table is presented in its entirety in a machine-readable form in the online journal. A portion is shown here for guidance regarding its form and content)

3.1. Stellar Parameters

To select the optimum template for each star from our library of synthetic spectra, we established the effective temperature, surface gravity, and metallicity from information in the literature and then ran grids of correlations to determine the best rotational velocity (as a proxy for spectral line broadening), as described in the previous section. We derived effective temperatures using published data for three sets of color indexes together with the calibrations from Ramirez & Melendez (2005). In those cases where metallicity values were available from McWilliam (1990) and Valdes et al. (2004), we used the effective temperature calibration corresponding to the published metallicity. For the other stars, we adopted a metallicity of $[Fe/H] = -0.15$, which is the mean for the stars with published values. The standard deviation from the mean for those stars is $\sigma[Fe/H] = \pm 0.17$, which corresponds to an uncertainty in effective temperature of about $\sigma T_{eff} = \pm 30$ K. We also assumed that the role of interstellar reddening was insignificant. For the color indexes, we used the visual broad bands $B-V$ and B_T-V_T from the Hipparcos Catalogue (ESA 1997); $V-J$, $V-H$, and $V-K$ using the infrared *JHK* magnitudes from 2MASS (Skrutskie et al. 2006); and the DDO narrow bands C(42-45) and C(42-48) from Mermilliod & Nitschelm (1989), when available. Many of the stars in our sample were too bright for the 2MASS instruments, so we only used the 2MASS photometry if the errors were less than 0.017, 0.016, and 0.015 mag in *JHK*, respectively. The agreement between $B-V$ and DDO temperatures is very good (generally within ±25 K at the 1σ level), while the agreement between these two and the *JHK* temperatures is not as good (generally about ±60 K at the 1σ level). Table 2 reports the color indexes that we used.

Next, we took advantage of the fact that all our stars had parallaxes measured by Hipparcos to derive bolometric luminosities, $L/L_\odot$, from the absolute V magnitudes using the bolometric corrections from VandenBerg & Clem (2003). Stellar radii were then obtained using the Stefan–Boltzmann law, $L = 4\pi R^2 \sigma T_{eff}^4$. Values for the log of the surface gravity, $\log g$, were taken from Allende Prieto & Lambert (1999) and McWilliam (1990) when available, and were estimated by comparison with theoretical evolutionary tracks (Girardi et al. 2000) for the other stars. Table 3 reports the Hipparcos distance in pc, our T_{eff} values and the standard deviation of the individual sets of values from the mean, σ_T, plus $\log(L/L_\odot)$, $R/R_\odot$, and $\log g$. When the total light of a binary or multiple was resolved into its individual components by the Hipparcos mission, the values reported in Table 3 refer to the giant component. Double-lined binaries are discussed separately in Section 4 and were thereby excluded from Table 3.

3.2. Macroturbulence and Stellar Rotation

Macroturbulence and stellar rotation affect the broadening of spectral lines differently, and the two effects can be separated using a Fourier analysis of spectra with very high spectral resolution and signal-to-noise ratio, as shown by Gray (1981). The spectra provided by the CfA Digital Speedometers have neither the spectral resolution nor the SNR to allow such an analysis. Thus we have chosen to determine the total observed line broadening using rotational broadening as a proxy, as described above. Then we correct for the macroturbulence expected for the luminosity and effective temperature of the star involved, based statistically on detailed measurements made by Gray & Nagar (1985), Gray & Toner (1986, 1987), and Gray (1989) using high-quality spectra.

Those authors reported the radial-tangential macroturbulence, ζ_{RT}, for each star they observed as a function of the star's spectral type and luminosity class. With the data now available to us, particularly the distances from Hipparcos for the stars they observed, we can render a more quantitative dependence

Table 4
Line Broadening Comparison with Measurements of Gray and Coworkers

				CfA			Gray		
Star	HR	$\log(L/L_\odot)$	$\log T_{\rm eff}$	$V_{\rm br}$	$\zeta_{\rm RT}$	$V_{\rm rot}$	$V_{\rm rot}$	$\zeta_{\rm RT}$	$V_{\rm br}$
HIP003031 . . .	163	1.62	3.704	4.5	5.1	1.8	2.5	6.3	5.6
HIP003179 . . .	168	2.88	3.657	10.2	7.1	8.5	4.9	6.2	6.9
HIP003419 . . .	188	2.13	3.681	7.3	5.6	5.8	3.0	5.9	5.6
HIP005951 . . .	373	1.57	3.696	5.9	4.8	4.5	4.5	5.6	6.3
HIP008198 . . .	510	2.07	3.691	5.6	5.9	3.1	2.9	4.9	4.9
HIP009884 . . .	617	1.91	3.653	5.2	4.0	4.2	3.1	3.9	4.4
HIP013531 . . .	854	2.05	3.725	7.2	7.9	3.5	3.6	6.5	6.3
HIP015900 . . .	1030	2.11	3.705	8.0	6.8	5.9	4.8	8.0	8.0
HIP020205 . . .	1346	1.87	3.691	6.0	5.1	4.4	2.4	5.9	5.3
HIP020252 . . .	1343	1.68	3.693	4.2	4.8	1.7	3.1	5.1	5.1
HIP020455 . . .	1373	1.83	3.688	7.0	4.9	5.8	2.5	6.2	5.5
HIP020885 . . .	1411	1.80	3.695	5.8	5.1	4.2	3.4	4.9	5.2
HIP020889 . . .	1409	1.95	3.681	5.9	5.1	4.3	2.5	6.2	5.5
HIP031592 . . .	2429	1.06	3.671	2.4	2.8	1.0	2.7	2.7	3.4
HIP037826 . . .	2990	1.54	3.685	4.3	4.2	2.7	2.5	4.2	4.2
HIP043813 . . .	3547	2.09	3.683	5.0	5.6	2.3	0.0	7.7	6.1
HIP046390 . . .	3748	3.10	3.605	9.5	5.3	8.5	0.0	6.5	5.2
HIP047908 . . .	3873	2.46	3.720	11.0	9.5	8.0	4.2	7.7	7.4
HIP050583 . . .	4057	2.42	3.640	5.7	5.3	3.9	2.6	5.2	4.9
HIP069673 . . .	5340	2.21	3.636	5.3	4.5	4.0	2.4	5.2	4.8
HIP072105 . . .	5506	2.70	3.658	12.1	6.8	10.8	6.6	9.3	9.9
HIP073555 . . .	5602	2.23	3.693	4.5	6.6	0.0	3.4	5.6	5.6
HIP074666 . . .	5681	1.70	3.690	5.1	4.8	3.5	1.1	5.7	4.7
HIP076219 . . .	5777	1.11	3.676	5.0	3.0	4.5	3.1	2.5	3.7
HIP077070 . . .	5854	1.75	3.653	5.1	3.6	4.3	0.0	4.8	3.8
HIP078132 . . .	5940	1.55	3.660	3.3	3.3	2.0	1.1	9.3	7.5
HIP080816 . . .	6148	2.18	3.689	5.7	6.3	2.8	3.4	6.8	6.4
HIP081833 . . .	6220	1.64	3.694	4.4	4.9	2.0	2.2	5.6	5.0
HIP086742 . . .	6603	1.80	3.652	6.1	3.6	5.4	1.6	4.0	3.6
HIP087933 . . .	6703	1.71	3.696	4.8	5.0	2.8	3.5	5.9	5.8
HIP088765 . . .	6770	1.85	3.691	4.0	5.2	0.0	3.9	4.3	5.2
HIP089918 . . .	6866	1.84	3.700	3.7	5.6	0.0	2.6	4.4	4.4
HIP089962 . . .	6869	1.24	3.687	3.8	3.7	2.4	2.8	2.5	3.4
HIP097118 . . .	7517	1.88	3.693	5.1	5.4	2.8	3.1	5.1	5.1
HIP100064 . . .	7754	1.59	3.691	4.5	4.5	2.7	3.2	4.6	4.9
HIP102488 . . .	7949	1.73	3.673	3.6	4.3	1.2	3.0	4.2	4.5
HIP102532 . . .	7948	1.30	3.678	4.5	3.3	3.6	2.8	3.4	3.9
HIP103004 . . .	7995	1.73	3.710	8.1	5.7	6.7	5.9	5.9	7.5
HIP104459 . . .	8093	1.57	3.692	3.3	4.5	0.0	2.8	4.6	4.6
HIP104732 . . .	8115	2.05	3.684	5.6	5.5	3.5	3.4	4.2	4.8
HIP105515 . . .	8167	1.87	3.700	8.4	5.7	7.0	5.6	6.2	7.5
HIP106481 . . .	8252	1.51	3.700	5.3	4.7	3.8	2.7	5.4	5.1
HIP112158 . . .	8650	2.38	3.708	6.6	8.1	1.4	2.8	6.0	5.5
HIP112529 . . .	8670	1.70	3.692	1.8	4.8	0.0	1.3	6.5	5.3
HIP112748 . . .	8684	1.67	3.694	5.5	4.8	4.0	2.6	4.2	4.2
HIP114273 . . .	8807	1.66	3.696	6.6	4.8	5.4	6.0	3.0	6.5
HIP114971 . . .	8852	1.68	3.698	3.2	5.0	0.0	0.0	5.5	4.4
HIP115919 . . .	8923	1.62	3.696	5.1	4.7	3.5	3.1	5.2	5.2
HIP117375 . . .	9012	1.67	3.694	3.2	4.8	0.0	1.2	6.0	4.9

Notes. To compare the total line broadening determined from the CfA spectra with the results obtained by Gray and coworkers for the same stars, we reconstructed the total line broadening for Gray's observations by adding their published values of $V_{\rm rot}$ and $\zeta_{\rm RT}$ in quadratures with the coefficient C_ζ in Equation (2) set to 0.63. The values for $\zeta_{\rm RT}$ used to correct the CfA observations for macroturbulence were derived using Equation (1), and thus match the typical value determined by Gray and coworkers at the same stellar parameters. The CfA values for $V_{\rm rot}$ were then calculated using $C_\zeta = 0.63$ in Equation (2). Column 3: log of the bolometric luminosity of the primary, in solar units $L_\odot$, Column 4: $T_{\rm eff}$ is in kelvin, Columns 5–10: all velocities are in km s^{-1}.

of macroturbulence on the stellar parameters. Our approach is illustrated in Figure 3, where we plot the individual stars from Gray & Nagar (1985), Gray & Toner (1986, 1987), and Gray (1989) on a diagram of $\log(L/L_\odot)$ versus $\log T_{\rm eff}$. The values of $\log T_{\rm eff}$ were derived using $B-V$ color temperatures, while $\log(L/L_\odot)$ was obtained in the same way as described above for our program stars. Both values are listed in Table 4. The dependence of macroturbulence on these two parameters is

Table 5
Line-Broadening Comparison with Measurements of Fekel

Star	HR	$\log(L/L_\odot)$	$\log T_{\mathrm{eff}}$	CfA			Fekel		
				V_{br}	ζ_{RT}	V_{rot}	V_{rot}	ζ_{RT}	V_{br}
HIP003419 . . .	188	2.13	3.681	7.3	5.6	5.8	4.0	3.0	5.0
HIP009884 . . .	617	1.91	3.653	5.2	4.0	4.2	1.8	3.0	3.5
HIP019388 . . .	1283	1.75	3.669	5.6	4.1	4.6	2.2	3.0	3.7
HIP026366 . . .	1907	1.45	3.690	3.0	4.1	0.0	0.4	3.0	3.0
HIP037740 . . .	2985	1.83	3.693	5.2	5.2	3.2	2.8	3.0	4.1
HIP037826 . . .	2990	1.54	3.685	4.3	4.2	2.7	1.7	3.0	3.4
HIP039311 . . .	3145	2.24	3.634	5.7	4.2	4.7	2.5	3.0	3.9
HIP040526 . . .	3249	2.94	3.601	7.9	4.8	6.9	4.0	3.0	5.0
HIP048356 . . .	3903	2.16	3.697	7.1	6.5	4.9	2.9	4.0	4.9
HIP058948 . . .	4608	1.79	3.685	2.2	4.8	0.0	2.5	3.0	3.9
HIP060172 . . .	4695	2.00	3.654	3.8	4.2	1.8	4.0	3.0	5.0
HIP063608 . . .	4932	1.82	3.696	1.9	5.3	0.0	3.2	3.0	4.4
HIP064022 . . .	4954	2.50	3.599	6.5	3.6	5.9	3.2	3.0	4.4
HIP069673 . . .	5340	2.21	3.636	5.3	4.5	4.0	3.3	3.0	4.5
HIP070755 . . .	5409	1.10	3.743	16.0	5.1	15.5	15.7	4.0	16.2
HIP076534 . . .	5823	1.24	3.701	2.1	4.0	0.0	0.6	2.0	2.1
HIP077655 . . .	5901	1.08	3.678	3.0	3.0	1.9	0.6	2.0	2.1
HIP078132 . . .	5940	1.55	3.660	3.3	3.3	2.0	2.2	2.0	3.0
HIP078159 . . .	5947	2.18	3.640	4.1	4.3	2.3	1.3	3.0	3.3
HIP079137 . . .	6014	0.61	3.679	1.2	2.3	0.0	0.6	2.0	2.1
HIP080816 . . .	6148	2.18	3.689	5.7	6.3	2.8	3.0	4.0	5.0
HIP086742 . . .	6603	1.80	3.652	6.1	3.6	5.4	2.5	3.0	3.9
HIP088765 . . .	6770	1.85	3.691	4.0	5.2	0.0	4.7	3.0	5.6
HIP089962 . . .	6869	1.24	3.687	3.8	3.7	2.4	2.6	2.0	3.3
HIP098110 . . .	7615	1.72	3.680	4.1	4.4	2.2	1.8	3.0	3.5
HIP102488 . . .	7949	1.73	3.679	3.6	4.3	1.2	2.0	3.0	3.6
HIP102532 . . .	7948	1.30	3.678	4.5	3.3	3.6	2.9	2.0	3.5
HIP110882 . . .	8551	1.50	3.672	3.2	3.7	1.4	1.0	3.0	3.2
HIP112997 . . .	8703	1.70	3.658	28.2	3.7	28.1	28.2	3.0	28.4

Notes. The total line broadening for Fekel (1997) was reconstructed using $C_\zeta = 0.5$ in Equation (2), Column 3: log of the bolometric luminosity of the primary, in solar units $L_\odot$, Column 4: T_{eff} is in kelvin, Columns 5–10: all velocities are in km s^{-1}.

reasonably fit by the empirical relation:

$$\log \zeta_{\mathrm{RT}} = 3.50 \log T_{\mathrm{eff}} + 0.25 \log(L/L_\odot) - 12.67. \quad (1)$$

Figure 4 displays the actual observed values of ζ_{RT} from Gray and collaborators compared to the values calculated with Equation (1). The rms residual of the observed from the fitted values is 1.0 km s^{-1}.

To extract the rotational velocity, $V_{\mathrm{rot}} \sin i$, from our observed line broadening, we subtracted the effects of macroturbulence in quadrature, as was done by Fekel (1997):

$$V_{\mathrm{rot}} \sin i = \left(V_{\mathrm{broad}}^2 - C_\zeta \zeta_{\mathrm{RT}}^2\right)^{1/2}. \quad (2)$$

For the coefficient C_ζ in this formula, Fekel (1997) adopted the value of 0.5 to take into account the difference in scale between the radial–tangential macroturbulence, ζ_{RT}, which is the quantity measured by Gray and collaborators, and the line broadening associated with the Doppler-shift distribution due to macroturbulence. The latter is a more appropriate quantity to subtract in quadrature from the total broadening. Because the macroturbulent velocity dispersion is not expected to be exactly Gaussian (Gray 1992), we chose instead to determine empirically the best value to use for C_ζ based on 49 stars in common. We used this procedure to subtract $\zeta_{\mathrm{RT}} = 1.5$ km s^{-1} and then add ζ_{RT} as calculated using Equation (1). We found that when we used $C_\zeta = 0.63$ to reconstruct the total line broadening from the $V_{\mathrm{rot}} \sin i$ and ζ_{RT} values published by Gray and collaborators, the average difference compared to our line broadening was minimized. We show this comparison for the 49 giants in common with Gray and collaborators in Figure 5, together with 29 stars in common with Fekel (1997). The broadening we observe seems to be systematically larger than Gray's only for stars of very high luminosity, $\log(L/L_\odot) > 2.45$, independently of T_{eff}. The rms residuals of our line-broadening values from the 45° line are ± 1.5 km s^{-1} using all 49 stars and ± 1.2 km s^{-1} using the 45 stars with $\log(L/L_\odot) < 2.45$. Our reconstruction of the total broadening measured by Fekel (1997) is documented in Table 5.

3.3. Mean Rotational and Radial Velocities and Error Estimates

The results of our velocity measurements for 748 giants with single-lined spectra are summarized in Table 6, where we give the number of observations, N_{obs}, the time spanned in days, the line broadening $\langle V_{\mathrm{br}} \rangle$, the inferred rotational velocity $\langle V_{\mathrm{rot}} \rangle$, the mean radial velocity on the native CfA system, and the uncertainty of the mean value. The uncertainty is either the standard deviation of the mean, i.e. the standard deviation of the individual velocities from the mean, ext, divided by the square root of the number of observations, or the average internal error estimate, int, divided by the square root of N_{obs},

Table 6
Mean Radial Velocities and Error Estimates for Stars with Single-Lined Spectra

Star	$N_{\rm obs}$	Span	$\langle V_{\rm br}\rangle$	$\langle V_{\rm rot}\rangle$	$\langle V_{\rm rad}\rangle$	±	ext	int	*e*/*i*	χ^2	P(χ^2)	⟨ht⟩
HIP000343 . . .	2	283	4.1	2.8	25.98	0.22	0.23	0.31	0.73	0.53	0.465280	0.958
HIP000443 . . .	3	93	2.1	0.0	−9.45	6.68	11.57	0.35	32.64	1932.69	0.000000	0.944
HIP000626 . . .	9	1151	4.8	3.8	−26.91	1.74	5.22	0.36	14.62	1745.30	0.000000	0.934
HIP000729 . . .	2	237	3.3	0.6	−20.23	0.21	0.20	0.30	0.68	0.47	0.493847	0.956
HIP000840 . . .	2	285	1.5	0.0	24.49	0.41	0.58	0.35	1.68	2.84	0.092191	0.954
HIP000873 . . .	2	244	1.4	0.0	8.39	0.23	0.21	0.33	0.65	0.43	0.510950	0.953
HIP001168 . . .	2	100	6.6	6.0	−46.26	0.57	0.80	0.57	1.40	1.97	0.160077	0.796
HIP001562 . . .	1	0	4.5	0.4	19.35	0.30	0.00	0.30	0.00	0.00	1.000000	0.959
HIP001640 . . .	2	15	2.9	1.9	9.68	0.22	0.04	0.32	0.12	0.02	0.900264	0.953
HIP001684 . . .	2	20	1.2	0.0	−19.97	0.23	0.33	0.33	1.00	1.01	0.315968	0.956
HIP002498 . . .	2	16	3.6	2.7	−13.30	0.23	0.30	0.33	0.91	0.83	0.362724	0.956
HIP002568 . . .	2	293	2.2	0.0	−12.07	0.20	0.02	0.28	0.09	0.01	0.930069	0.965
HIP003031 . . .	3	407	4.5	2.0	−84.43	0.20	0.26	0.35	0.76	1.12	0.571506	0.946
HIP003092 . . .	63	4190	7.0	6.5	−9.88	0.15	1.19	0.44	2.71	456.56	0.000000	0.918

Notes. Column 1: star name from Hipparcos, Column 2: number of observations, Column 3: time spanned (days), Column 4: observed spectral line broadening (km s^{-1}), Column 5: derived projected rotational velocity (km s^{-1}), Column 6: mean radial velocity for single-lined spectra (km s^{-1}), Column 7: error in the mean velocity (km s^{-1}), Column 8: external rms residuals in the observed velocities (km s^{-1}), Column 9: internal velocity error estimate (km s^{-1}), Column 10: ratio of external to internal errors, Column 11: χ^2, Column 12: χ^2 probability, Column 13: mean of the peak correlation height.
(This table is presented in its entirety in a machine-readable form in the online journal. A portion is shown here for guidance regarding its form and content)

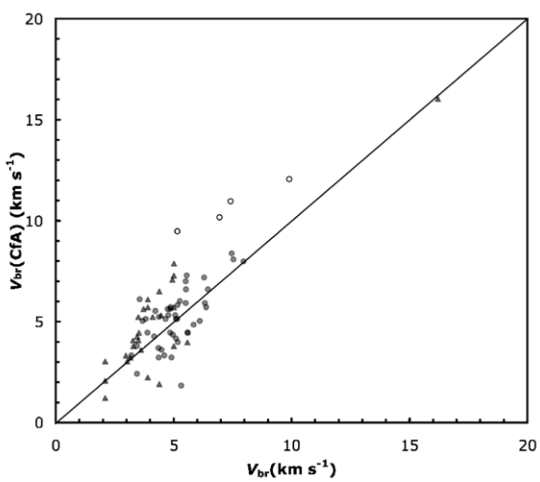

Figure 5. Total line broadening measured at CfA for 49 stars in common with Gray and coworkers and 29 in common with Fekel (1997). Stars in the first group are plotted as filled circles for $\log(L/L_{\odot}) < 2.45$ and as open circles for $\log(L/L_{\odot}) > 2.45$, while the second group is plotted as filled triangles. The reconstruction of the total line broadening used for Gray and Fekel is documented in Tables 4 and 5, respectively.

whichever error is larger. Next, we report *e*/*i*, the ratio of the external to internal error, and then χ^2 and the probability of getting a χ^2 value this big or larger just by chance for a star that is actually constant and errors that are Gaussian (e.g., see Carney et al. 2003). In our experience, stars with χ^2 values smaller than 0.001 often prove to be spectroscopic binaries. In the final column, we give the average value of the peak correlation height.

In Table 7, we report the individual radial velocities and internal error estimates for the single-lined stars summarized in Table 6. In our sample, 13 of the 761 giants show composite spectra. Tables 8 and 9 report the individual velocities for twelve double-lined and one triple-lined system, respectively. $V_{\rm B}$ and $V_{\rm C}$ are the velocities for the secondary and tertiary components. The single-lined velocities were derived using **rvsao** (Kurtz & Mink 1998) running inside the IRAF[5] environment. The double-lined velocities were derived using TODCOR (Zucker & Mazeh 1994) as implemented at CfA by Guillermo Torres. To derive all three velocities for the triple-lined system HIP 109281, we used the three-dimensional correlation tool TRICOR as implemented at CfA by Guillermo Torres.

Table 7
Single-Lined Radial Velocities

Star	Tel	Template	HJD	$V_{\rm A}$	$\sigma(V_{\rm A})$
HIP000343	W	t04750g25p00v002	245 2962.536 51	25.82	0.18
HIP000343	W	t04750g25p00v002	245 3245.776 95	26.14	0.20
HIP000443	W	t04750g30m05v001	245 3284.644 57	−18.83	0.23
HIP000443	W	t04750g30m05v001	245 3339.577 33	−12.99	0.21
HIP000443	W	t04750g30m05v001	245 3378.461 25	3.47	0.31
HIP000626	W	t04750g30p00v004	245 2978.564 61	−19.40	0.24
HIP000626	W	t04750g30p00v004	245 3247.722 38	−20.66	0.20
HIP000626	W	t04750g30p00v004	245 3320.690 17	−22.46	0.20
HIP000626	W	t04750g30p00v004	245 3400.479 76	−24.04	0.20
HIP000626	T	t04750g30p00v004	245 3718.615 44	−30.99	0.28
HIP000626	T	t04750g30p00v004	245 3749.592 30	−31.79	0.36

Notes. Column 1: star name from Hipparcos, Column 2: telescope (W: Wyeth, T: Tillinghast, M: MMT), Column 3: template (see text for code), Column 4: heliocentric Julian date, Column 5: heliocentric radial velocity (km s^{-1}), Column 6: radial velocity error estimate (km s^{-1}).
(This table is presented in its entirety in a machine-readable form in the online journal. A portion is shown here for guidance regarding its form and content)

For each velocity, the synthetic spectrum that was used as the template is designated by a code, where the “t” field specifies the effective temperature, the “g” field gives ten times log *g*, and the “m” or “p” fields report the metallicity, [Fe/H], also multiplied by 10, with “m” standing for minus and “p” for positive values. The “v” field specifies the rotational velocity. The telescope codes are “W” for the 1.5 m Wyeth Reflector at the Oak Ridge Observatory, “T” for the 1.5 m Tillinghast

[5] IRAF (Interactive Reduction and Analysis Facility) is distributed by the National Optical Astronomy Observatory, which is operated by the Association of Universities for Research in Astronomy, Inc., under cooperative agreement with the National Science Foundation.

Table 8
Double-Lined Radial Velocities

Star	Template A	Template B	HJD	V_A	V_B
HIP004463	t05000g25p00v006	t05000g25p00v006	244 515 96.4723	5.94	−27.25
HIP004463	t05000g25p00v006	t05000g25p00v006	244 517 15.8360	3.33	−25.85
HIP004463	t05000g25p00v006	t05000g25p00v006	244 517 54.8656	−27.29	7.62
HIP004463	t05000g25p00v006	t05000g25p00v006	244 517 76.8265	−22.47	1.12
HIP004463	t05000g25p00v006	t05000g25p00v006	244 517 96.7528	−3.43	−15.99
HIP004463	t05000g25p00v006	t05000g25p00v006	244 518 57.7099	−20.64	−2.21
HIP004463	t05000g25p00v006	t05000g25p00v006	244 518 78.5848	−28.62	8.05
HIP004463	t05000g25p00v006	t05000g25p00v006	244 518 99.6052	−16.18	−2.83
HIP004463	t05000g25p00v006	t05000g25p00v006	244 519 27.5150	6.49	−27.15
HIP004463	t05000g25p00v006	t05000g25p00v006	244 519 48.4851	2.03	−25.51
HIP004463	t05000g25p00v006	t05000g25p00v006	244 519 65.4669	−13.51	−8.35
HIP004463	t05000g25p00v006	t05000g25p00v006	244 520 80.8165	−10.47	−10.50
HIP004463	t05000g25p00v006	t05000g25p00v006	244 521 14.8611	−28.23	6.31

Notes. Column 1: star name from Hipparcos, Column 2: template for primary, Column 3: template for secondary, Column 4: heliocentric Julian date, Column 5: primary heliocentric radial velocity (km s^{-1}), Column 6: secondary heliocentric radial velocity (km s^{-1}).
(This table is presented in its entirety in a machine-readable form in the online journal. A portion is shown here for guidance regarding its form and content)

Table 9
Triple-Lined Radial Velocities

Star	Template A	Template B	Template C	HJD	V_A	V_B	V_C
HIP109281	t05000g30p00v010	t05000g30p00v000	t06000g45p00v000	244 529 67.5719	28.40	12.40	2.10
HIP109281	t05000g30p00v010	t05000g30p00v000	t06000g45p00v000	244 530 03.4789	6.50	7.80	27.20
HIP109281	t05000g30p00v010	t05000g30p00v000	t06000g45p00v000	244 531 83.7636	6.40	7.30	28.60
HIP109281	t05000g30p00v010	t05000g30p00v000	t06000g45p00v000	244 532 16.7807	26.20	11.40	4.50
HIP109281	t05000g30p00v010	t05000g30p00v000	t06000g45p00v000	244 532 35.7793	7.30	7.60	23.80
HIP109281	t05000g30p00v010	t05000g30p00v000	t06000g45p00v000	244 532 42.6450	6.80	7.20	28.30
HIP109281	t05000g30p00v010	t05000g30p00v000	t06000g45p00v000	244 532 50.6847	7.40	7.60	26.10
HIP109281	t05000g30p00v010	t05000g30p00v000	t06000g45p00v000	244 532 62.7044	26.20	10.70	4.50
HIP109281	t05000g30p00v010	t05000g30p00v000	t06000g45p00v000	244 532 78.6020	22.80	11.80	5.20
HIP109281	t05000g30p00v010	t05000g30p00v000	t06000g45p00v000	244 532 97.5022	6.90	7.40	26.40
HIP109281	t05000g30p00v010	t05000g30p00v000	t06000g45p00v000	244 533 05.5506	6.60	7.00	29.20
HIP109281	t05000g30p00v010	t05000g30p00v000	t06000g45p00v000	244 533 13.5270	9.10	9.30	21.60
HIP109281	t05000g30p00v010	t05000g30p00v000	t06000g45p00v000	244 533 21.4916	25.70	11.10	4.90
HIP109281	t05000g30p00v010	t05000g30p00v000	t06000g45p00v000	244 533 29.4917	31.40	10.30	−0.10
HIP109281	t05000g30p00v010	t05000g30p00v000	t06000g45p00v000	244 533 48.5866	9.90	10.00	18.90
HIP109281	t05000g30p00v010	t05000g30p00v000	t06000g45p00v000	244 533 57.4718	7.10	7.40	28.00
HIP109281	t05000g30p00v010	t05000g30p00v000	t06000g45p00v000	244 533 89.4479	31.10	9.70	−0.90
HIP109281	t05000g30p00v010	t05000g30p00v000	t06000g45p00v000	244 534 75.8803	7.20	7.50	28.50
HIP109281	t05000g30p00v010	t05000g30p00v000	t06000g45p00v000	244 536 59.7361	5.80	6.20	29.00
HIP109281	t05000g30p00v010	t05000g30p00v000	t06000g45p00v000	244 537 23.5651	5.70	5.80	27.40
HIP109281	t05000g30p00v010	t05000g30p00v000	t06000g45p00v000	244 539 22.9362	30.20	7.20	1.80
HIP109281	t05000g30p00v010	t05000g30p00v000	t06000g45p00v000	244 539 28.9652	25.40	8.80	1.40
HIP109281	t05000g30p00v010	t05000g30p00v000	t06000g45p00v000	244 539 84.8190	29.05	6.00	3.00
HIP109281	t05000g30p00v010	t05000g30p00v000	t06000g45p00v000	244 540 72.5369	5.60	6.10	30.50
HIP109281	t05000g30p00v010	t05000g30p00v000	t06000g45p00v000	244 542 83.8773	25.90	9.20	1.60

Notes. Column 1: star name from Hipparcos, Column 2: template for primary, Column 3: template for secondary, Column 4: template for tertiary, Column 5: heliocentric Julian date, Column 6: primary heliocentric radial velocity (km s^{-1}), Column 7: secondary heliocentric radial velocity (km s^{-1}), Column 8: tertiary heliocentric radial velocity (km s^{-1}).

Reflector at the Whipple Observatory, and “M” for the MMT at the Whipple Observatory.

All of the CfA velocities reported in this paper are on the CfA native system. To put these velocities onto an absolute system defined by minor-planet observations 0.139 km s^{-1} must be added to the native velocities. No attempt has been made to correct for differences in gravitational redshift between the solar spectrum used to calibrate the CfA velocity zero point and the spectra of the giants studied here.

4. SPECTROSCOPIC BINARIES

Our observational strategy proceeded in two stages. Initially we obtained a well-exposed spectrum suitable for determining the line broadening. In most cases, we followed this up with a second exposure, to check the first observation. If the line broadening from the initial pair of exposures of a star turned out to be less than 5 km s^{-1}, in most cases we did not schedule additional observations. For those stars with more

Table 10
CfA Single-Lined Orbital Solutions

Star	P	γ	K	e	ω	T	$a_A \sin i$	$f(m)$	N σ	Span Cycles
HIP000626 . . .	1568.	−25.92	6.87	0.06	273.	54276.	148.	0.0523	9	1151.0
	±239.	±0.46	±0.41	±0.12	±104.	±377.	±16.	±0.0051	±0.46	0.7
HIP003693 . . .	17.7674	−24.38	25.26	0.013	77.	53266.2	6.17	0.0297	17	382.9
	±0.0048	±0.21	±0.31	±0.011	±52.	±2.6	±0.12	±0.0017	±0.76	21.6
HIP011840 . . .	629.2	+2.729	10.67	0.135	294.6	53979.	91.45	0.0770	9	1182.9
	±2.7	±0.096	±0.13	±0.015	±6.5	±10.	±0.50	±0.0013	±0.23	1.9
HIP020455 . . .	532.0	+38.598	2.904	0.415	351.1	50263.8	19.33	0.001018	61	7296.9
	±1.4	±0.055	±0.076	±0.022	±4.3	±5.3	±0.43	±0.000067	±0.41	13.7
HIP020885 . . .	6091.	+39.293	7.44	0.597	65.1	50999.	499.8	0.1341	42	5583.0
	±156.	±0.082	±0.14	±0.013	±2.2	±18.	±9.6	±0.0057	±0.43	0.9
HIP022055 . . .	680.	+25.90	6.48	0.102	42.	53797.	60.3	0.0189	11	1219.8
	±10.	±0.51	±0.41	±0.097	±30.	±52.	±3.7	±0.0033	±0.50	1.8
HIP022176 . . .	107.57	+43.28	8.51	0.252	254.5	49457.5	12.19	0.00623	18	1505.9
	±0.12	±0.11	±0.15	±0.019	±4.2	±1.2	±0.19	±0.00029	±0.45	14.0
HIP023221 . . .	898.1	−15.749	5.20	0.173	155.1	51240.	63.2	0.01248	35	4435.1
	±2.7	±0.092	±0.14	±0.025	±8.2	±21.	±1.6	±0.00095	±0.49	4.9
HIP023896 . . .	930.	−15.45	8.31	0.114	169.	53622.	105.5	0.0542	8	1222.9
	±11.	±0.43	±0.85	±0.050	±18.	±50.	±4.1	±0.0066	±0.21	1.3
HIP025282 . . .	1496.	+21.18	1.98	0.60	338.7	50249.	33.	0.00061	47	8608.5
	±15.	±0.15	±0.74	±0.11	±8.2	±45.	±10.	±0.00059	±0.55	5.8
HIP037629 . . .	19.60437	+43.043	34.776	0.0143	46.	53507.96	9.374	0.08540	78	1252.8
	±0.00053	±0.066	±0.100	±0.0026	±13.	±0.71	±0.024	±0.00066	±0.45	63.9
HIP039198 . . .	365.42	−4.23	9.56	0.515	108.1	53826.9	41.15	0.02080	17	1272.8
	±0.57	±0.16	±0.17	±0.018	±3.2	±1.3	±0.54	±0.00082	±0.43	3.5
HIP040221 . . .	76.364	−27.97	12.97	0.449	153.1	53868.89	12.17	0.01233	16	1237.8
	±0.030	±0.13	±0.18	±0.013	±1.9	±0.35	±0.18	±0.00056	±0.50	16.2
HIP041935 . . .	324.	+16.53	3.83	0.149	90.	54051.	16.9	0.00183	10	1190.0
	±10.	±0.41	±0.34	±0.096	±54.	±59.	±1.4	±0.00051	±0.54	3.7
HIP050801 . . .	230.39	−21.44	7.82	0.103	191.	53764.	24.64	0.0112	12	1270.9
	±0.52	±0.15	±0.23	±0.027	±18.	±12.	±0.73	±0.0010	±0.50	5.5
HIP052085 . . .	1319.	+17.45	3.54	0.27	163.	51353.	62.	0.0054	18	6265.0
	±31.	±0.70	±0.43	±0.19	±18.	±39.	±11.	±0.0031	±0.61	4.7
HIP057565 . . .	71.692	+0.34	30.08	0.0039	239.	48837.	29.66	0.2022	12	1551.9
	±0.012	±0.13	±0.20	±0.0065	±122.	±24.	±0.16	±0.0034	±0.42	21.6
HIP057791 . . .	489.55	+15.51	12.48	0.2200	102.4	53114.4	81.97	0.0916	9	1800.1
	±0.97	±0.12	±0.17	±0.0073	±3.2	±4.2	±0.39	±0.0013	±0.17	3.7
HIP060351 . . .	396.9	−0.5	26.4	0.623	105.5	53224.9	113.	0.36	17	2183.1
	±1.4	±1.1	±4.1	±0.051	±7.2	±4.4	±14.	±0.14	±0.62	5.5
HIP061910S . . .	44.508	−10.53	27.57	0.278	249.3	53695.02	16.21	0.0857	29	1283.8
	±0.010	±0.25	±0.29	±0.012	±2.5	±0.35	±0.33	±0.0053	±1.01	28.8
HIP066511 . . .	47.9499	−48.29	30.82	0.0369	196.2	53083.1	20.31	0.1451	16	1205.7
	±0.0058	±0.12	±0.22	±0.0067	±10.0	±1.3	±0.12	±0.0027	±0.44	25.1
HIP069879 . . .	212.24	−20.86	19.35	0.540	226.3	53859.63	47.52	0.0949	14	1207.0
	±0.18	±0.17	±0.62	±0.017	±1.9	±0.76	±0.99	±0.0058	±0.47	5.7
HIP072706 . . .	83.556	−46.326	25.16	0.5028	274.93	53300.24	24.985	0.0890	16	430.8
	±0.042	±0.093	±0.19	±0.0066	±0.80	±0.18	±0.096	±0.0010	±0.32	5.2
HIP074896 . . .	508.7	−7.743	6.19	0.327	39.0	53751.8	40.90	0.01053	38	1246.9
	±1.6	±0.074	±0.12	±0.016	±3.4	±4.0	±0.67	±0.00051	±0.44	2.5
HIP075325 . . .	11.13413	+61.90	39.52	0.021	45.	48278.26	6.05	0.0711	38	2578.9
	±0.00036	±0.32	±0.45	±0.012	±31.	±0.96	±0.27	±0.0095	±1.94	231.6
HIP078481 . . .	1277.	−18.71	3.90	0.310	131.	54655.	65.0	0.00673	15	1379.3
	±89.	±0.25	±0.19	±0.055	±12.	±104.	±4.8	±0.00094	±0.42	1.1
HIP080816 . . .	413.1	−25.91	12.32	0.586	19.7	53310.9	56.7	0.0426	10	1108.1
	±5.1	±0.54	±0.44	±0.036	±4.6	±9.3	±3.0	±0.0077	±0.53	2.7
HIP083138 . . .	900.	−13.65	3.36	0.070	338.	52956.	41.5	0.00352	13	1323.3
	±14.	±0.20	±0.16	±0.068	±50.	±114.	±1.3	±0.00031	±0.31	1.5
HIP084402 . . .	2348.7	−7.406	9.113	0.4128	119.35	53191.1	268.08	0.13917	8	2128.2
	±7.5	±0.040	±0.065	±0.0038	±0.99	±3.7	±0.10	±0.00019	±0.03	0.9
HIP090135 . . .	2303.33	−5.017	7.636	0.0680	313.6	54441.	241.2877	0.1055055	7	2160.2
	±0.87	±0.019	±0.033	±0.0011	±1.7	±11.	±0.0054	±0.0000075	±0.00	0.9
HIP110900 . . .	1505.	+4.79	6.22	0.370	73.	49171.	119.6	0.0301	18	4188.6
	±24.	±0.15	±0.49	±0.037	±14.	±35.	±6.8	±0.0057	±0.49	2.8

Table 10
(Continued)

Star	P	γ	K	e	ω	T	$a_A \sin i$	$f(m)$	N σ	Span Cycles
HIP112158 . . .	813.	+4.17	14.37	0.183	344.7	52025.	158.0	0.238	14	1743.3
	±22.	±0.35	±0.37	±0.024	±8.8	±30.	±4.2	±0.018	±0.65	2.1
HIP112997 . . .	24.64784	−13.594	33.376	0.0068	212.	50844.3	11.312	0.0949	202	2404.6
	±0.00028	±0.062	±0.087	±0.0026	±22.	±1.5	±0.051	±0.0013	±0.87	97.6
HIP116584 . . .	20.5233	+6.496	6.578	0.075	322.	50112.59	1.851	0.000600	82	2537.1
	±0.0019	±0.068	±0.097	±0.014	±11.	±0.65	±0.033	±0.000032	±0.60	123.6
HIP028734B . . .	9.59697	+27.59	52.15	0.014	166.	53240.29	6.88	0.1410	18	464.8
	±0.00080	±0.29	±0.40	±0.009	±32.	±0.85	±0.13	±0.0077	1.18	48.4

Notes. Column 2: period P in days, Column 3: center-of-mass velocity γ in km s^{-1}, Column 4: projected orbital semiamplitude of the primary K in km s^{-1}, Column 5: eccentricity e, Column 6: angle of periastron ω in degrees, Column 7: heliocentric Julian Date −2400,000 for periastron passage T, Column 8: projected semimajor axes of the primary $a \sin i$ in GM, Column 9: mass function $f(m)$ in $M_\odot$, Column 10: number of velocities and rms velocity residuals in km s^{-1}, Column 11: time spanned by the observations in days and number of orbital cycles covered.

than 5 km s^{-1} of line broadening, our goal was to obtain enough additional exposures to identify spectroscopic binaries with periods shorter than a few hundred days. Our plan was to accumulate enough spectra to allow orbital solutions for these binaries, but the Oak Ridge Observatory was abruptly shut down before we could achieve that goal. It turns out that this was not a complete disaster, because published orbital solutions were already available for many of the binaries in our sample, and we were able to obtain additional velocities for critical binaries using the CfA Digital Speedometer on the 1.5 m Tillinghast Reflector at the Whipple Observatory.

Our techniques for identifying spectroscopic binaries were similar to those described in Latham et al. (2002) and will not be repeated in detail here. To summarize, we inspected each spectrum and a plot of its correlation function to look for composite spectra. This led to the identification of 12 double-lined binaries, a triple-lined hierarchical triple system (HIP 109281), a double-lined hierarchical triple system (HIP 28734), and a double-lined binary (HIP 61910N) in a quadruple system with a single-lined binary (HIP 61910S). For the stars showing only one set of lines, we calculated the probability that the observed χ^2 was due to Gaussian errors for a star with constant velocity, and scrutinized more carefully those cases where the probability was less than 1%. We also reviewed plots of the velocity history and power spectrum for each star.

In Table 10, we report the results of our orbital solutions for 35 single-lined binaries, one of which is the inner binary in the triple system HIP 28734, and in Table 11 the orbital parameters for 12 double-lined binaries, one of which is the inner binary in the triple system HIP 109281. The corresponding velocity curves and individual velocity observations are plotted in Figures 6 and 7.

Because the nearby giants in our sample are bright, many of them have published orbits, with some of the solutions dating back almost 100 years. For example, the 9th Catalogue of Spectroscopic Binary Orbits (Pourbaix et al. 2004, hereafter SB9) reports single-lined orbital solutions for 60 of the stars in our sample and double-lined solutions for 16 of the stars. Unfortunately, in many cases SB9 does not report errors for the orbital parameters, often because the original publication did not estimate the errors. Therefore, we reviewed the literature for binaries with published orbits, deriving new orbital solutions with error estimates where appropriate, and including new velocities from CfA and other sources when available. The key orbital parameters for these binaries are reported in Tables 12 and 13. The full details for these orbits will be submitted to SB9 and thus they are not documented here.

4.1. Tidal Circularization

Close binaries are subject to tidal interactions that tend to synchronize the rotational periods with the orbital periods and to circularize the orbits, normally with the sequence of events in this order (Zahn 1977, 1989, 1992). For most binaries in the solar neighborhood with orbital periods longer than about 10 days, the stellar radii are too small for tidal circularization to be important as long as both stars are on the main sequence (e.g., see Duquennoy & Mayor 1991; Mathieu et al. 1992; Latham et al. 2002). When the more massive primary star begins to evolve away from the main sequence, its radius swells, the convective envelope grows, and tidal torques can become important. The time scale for tidal circularization can be very short compared to the evolutionary time scale of the primary, because the tidal torques depend very strongly on the ratio of stellar radius to the separation of the two stars.

The location of our 79 giants in 75 binary systems with orbital solutions on a $\log T_{\rm eff}$ versus $\log(L/L_\odot)$ diagram is shown in Figure 8, together with Girardi et al. (2000) representative evolutionary tracks for stars with mass 1.0, 1.4, 1.8, 2.2, 3.0 $M_\odot$ and metallicity [Fe/H] = −0.2, which is close to the average value in the solar neighborhood (e.g., see McWilliam 1990; Nordström et al. 2004). In the region of the diagram where the tracks for different masses and evolutionary stages overlap, one cannot distinguish between stars that are on the first ascent up the giant branch (FA) and stars that have already passed the tip of the giant branch (PT) and are now either on the horizontal branch (HB) or the asymptotic giant branch (AGB). The determination of mass and age for these stars is therefore ambiguous.

Figures 9 and 10 display the orbital eccentricity and the measured $V_{\rm rot} \sin i$ as a function of the orbital period P for the binaries in our sample. In both figures, the filled circles are used for stars unambiguously in the first ascent, while open circles are used for systems of ambiguous evolutionary stage, as defined in Figure 8. For all the binaries in our sample with periods shorter than 20 days the orbits have been circularized, while about half the orbits with periods in the range 20–100 days still show significant eccentricity. All of the eccentric orbits with periods shorter than 120 days are unambiguously on the first ascent. This is not surprising, because the process of circularization strongly depends on the stellar radius, and the average radius of the stars in the first ascent subsample is smaller than that of the

Table 11
CfA Double-Lined Orbital Solutions

Star	P q	γ	K_A K_B	e	ω	T	$a_A \sin i$ $a_B \sin i$	$M_A \sin^3 i$ $M_B \sin^3 i$	N σ	Span Cycles
HIP004463 ...	115.733	−10.52	17.98	0.0032	103.	52662.	28.61	0.3127	62	2422.3
	±0.023	±0.06	±0.09	±0.0044	±75.	±24.	±0.15	±0.0042	0.55	20.9
	0.9446	...	19.03	...	...	...	30.29	0.2954	62	...
	±0.0073	...	±0.11	...	...	...	±0.18	±0.0036	0.70	...
HIP004592 ...	58.700	−16.14	37.04	0.2261	118.7	53590.21	29.13	1.108	16	1310.4
	±0.012	±0.15	±0.21	±0.0072	±1.4	±0.25	±0.18	±0.031	0.55	22.3
	1.016	...	36.47	...	...	...	28.67	1.125	16	...
	±0.014	...	±0.43	...	...	...	±0.38	±0.022	1.33	...
HIP010280A ...	14.73018	−19.49	54.84	0.0035	29.	53353.0	11.112	1.065	22	743.0
	±0.00089	±0.16	±0.36	±0.0042	±65.	±2.7	±0.079	±0.015	1.12	50.4
	0.9729	...	56.39	...	...	...	11.422	1.036	22	...
	±0.0086	...	±0.29	...	...	...	±0.065	±0.016	0.87	...
HIP016042 ...	6.43781	22.29	61.53	0.0028	149.	53258.4	5.447	0.7434	17	416.9
	±0.00016	±0.15	±0.57	±0.0028	±62.	±1.1	±0.056	±0.0091	1.88	64.8
	0.9153	...	67.22	...	...	...	5.951	0.680	17	...
	±0.0097	...	±0.19	...	...	...	±0.019	±0.014	0.52	...
HIP047508 ...	14.49800	26.19	54.78	0.0022	230.	53132.8	10.920	1.260	18	1437.0
	±0.00048	±0.17	±0.28	±0.0048	±101.	±4.2	±0.062	±0.024	0.78	99.1
	0.8869	...	61.76	...	...	...	12.31	1.118	18	...
	±0.0091	...	±0.48	...	...	...	±0.11	±0.016	1.38	...
HIP061910N ...	1.460866	−10.8	100.3	0.211	82.1	53981.369	1.969	1.055	29	1283.8
	±0.000020	±1.8	±3.1	±0.024	±6.8	±0.026	±0.063	±0.092	11.20	878.8
	0.743	...	134.9	...	...	...	2.65	0.784	29	...
	±0.037	...	±5.0	...	...	...	±0.10	±0.059	17.97	...
HIP076563 ...	3.273167	−34.35	85.67	0.0114	287.3	53309.905	3.8556	0.8852	40	1260.5
	±0.000020	±0.10	±0.18	±0.0017	±8.3	±0.076	±0.0087	±0.0050	0.86	385.1
	0.9815	...	87.28	...	...	...	3.928	0.8689	40	...
	±0.0033	...	±0.21	...	...	...	±0.010	±0.0045	0.99	...
HIP078259 ...	9.01538	−5.98	53.16	0.0000	...	53197.2848	6.591	0.8841	21	232.6
	±0.00056	±0.10	±0.13	Fixed	...	±0.0036	±0.015	±0.0095	0.42	25.8
	0.8017	...	66.31	...	...	...	8.221	0.7088	21	...
	±0.0048	...	±0.31	...	...	...	±0.042	±0.0050	1.12	...
HIP096683 ...	434.208	4.502	26.40	0.5557	209.41	51239.58	131.07	2.0242	291	1634.8
	±0.046	±0.019	±0.05	±0.0009	±0.13	±0.10	±0.22	±0.0085	0.42	3.8
	0.9699	...	27.22	...	...	...	135.14	1.9633	291	...
	±0.0024	...	±0.06	...	...	...	±0.26	±0.0075	0.50	...
HIP104987 ...	98.809	−16.26	15.81	0.0069	42.	52717.	21.48	0.2339	108	2509.3
	±0.014	±0.06	±0.07	±0.0053	±40.	±11.	±0.10	±0.0051	0.61	25.4
	0.8348	...	18.93	...	...	...	25.72	0.1953	108	...
	±0.0094	...	±0.19	...	...	...	±0.26	±0.0028	1.62	...
HIP109281 ...	59.331	16.22	13.03	0.237	318.0	53442.09	10.33	0.0696	25	1316.3
	±0.031	±0.16	±0.25	±0.018	±4.4	±0.61	±0.20	±0.0053	0.79	22.2
	0.849	...	15.34	...	...	...	12.16	0.0592	25	...
	±0.032	...	±0.51	...	...	...	±0.42	±0.0033	1.88	...
HIP116243 ...	94.851	−40.54	36.21	0.5169	315.82	53555.40	40.43	1.67	12	1250.5
	±0.013	±0.16	±0.75	±0.0099	±0.54	±0.13	±0.67	±0.15	0.24	13.2
	0.841	...	43.04	...	...	...	48.1	1.403	12	...
	±0.033	...	±1.58	...	...	...	±1.9	±0.085	2.69	...

Notes. Column 2: period P in days, mass ratio $q = M_{mB}/M_{mA}$, Column 3: center-of-mass velocity γ in km s^{-1}, Column 4: projected orbital velocities of the primary and secondary K_A and K_B in km s^{-1}, Column 5: eccentricity e, Column 6: angle of periastron ω in degrees, Column 7: heliocentric Julian Date −2400,000 for periastron passage T, Column 8: projected semimajor axes of the primary and secondary $a_A \sin i$ and $a_B \sin i$ in GM, Column 9: projected masses of the primary and secondary $M_A \sin^3 i$ and $M_B \sin^3 i$ in $M_\odot$, Column 10: number of velocities and rms velocity residuals in km s^{-1} for the primary and secondary, and Column 11: time spanned by the observations in days and number of orbital cycles covered.

ambiguous subsample. All binaries with a period shorter than about 30 days and about half of those with periods between 30 and 120 days appear to be synchronized.

In Tables 14 and 15, we display the main physical parameters that we infer for these stars. These parameters include log $T_{\rm eff}$, $\log(L/L_\odot)$, $R/R_\odot$, and mass. For the stellar mass, the tables include values corresponding to tracks on the first ascent $M_{\rm FA}/M_\odot$ and post-tip $M_{\rm PT}/M_\odot$: both values are reported for stars whose evolutionary stage is ambiguous. In determining stellar masses, we took into account metallicity when possible and otherwise used the sample average. In the case of double-lined binaries observed at CfA, we adopted the effective temperature for the secondary that gave the best correlations in our TODCOR (Zucker & Mazeh 1994) analysis of our observed spectra. We then subtracted the contribution of the secondary from the total observed V and $B - V$ (using the light ratio from our TODCOR

Table 12
Single-Lined Orbits Using Published Velocities

Star	P	σ_P	e	σ_e	K	σ_K	Ref.
HIP000443 . . .	72.93	. . .	0.272	0.017	16.43	0.31	4, 00
. . .	72.9404	0.0013	0.261	0.017	16.73	0.33	4, 10, 31, 000
HIP003092 . . .	21022	401	0.512	0.036	4.48	0.20	21, 22, 23, 24, 10, 000
HIP003675 . . .	843	4	0.386	0.013	5.277	0.001	62, 00
HIP003693 . . .	17.769426	0.000040	0	Fixed	25.11	0.15	5, 00
HIP005951 . . .	56.824	0.011	0.00	Fixed	7.13	0.13	6, 00
. . .	56.9	0.1	0.02	. . .	7.11	0.47	66, 00
HIP007143 . . .	36.588	0.024	0.203	0.031	29.97	0.88	7, 00
. . .	36.598	0.034	0.189	0.051	30.0	1.5	7, 0
. . .	36.355	0.001	0.111	0.035	32.03	1.11	7, 10, 000
HIP007719 . . .	7581	48	0.368	0.020	3.01	0.09	20, 00
HIP008645 . . .	1549	24	0.560	0.070	3.31	0.30	25, 0
. . .	1631.6	1.5	0.648	0.038	3.83	0.23	25, 26, 10, 27, 000
HIP008833 . . .	1672.4	1.4	0.18	0.03	4.64	0.14	28, 00
HIP010366 . . .	1575.5	1.6	0.8815	0.0010	20.37	0.09	2, 00
HIP011840 . . .	619.22	0.29	0.115	0.034	11.04	0.42	30, 000
HIP013531 . . .	1515.81	0.05	0.729	0.004	18.97	0.20	29, 00
HIP015900 . . .	1654.9	2.4	0.263	0.029	4.39	0.16	15, 00
. . .	1654.1	1.2	0.271	0.036	4.41	0.18	15, 30, 32, 000
HIP020455 . . .	529.8	0.3	0.42	0.06	3.0	0.2	33, 00
. . .	522.1	1.8	0.48	. . .	2.84	0.03	67, 00
HIP020855 . . .	5939	46	0.570	0.022	7.17	0.51	63. 00
HIP022176 . . .	107.503	0.023	0.210	0.017	8.51	0.15	34, 00
HIP023221 . . .	895.4	1.6	0.259	0.045	4.81	0.22	35, 10, 000
HIP024727 . . .	434.161	0.055	0.108	0.021	14.74	0.31	10, 26, 30, 32, 000
HIP025282 . . .	1520	17	0.55	0.12	1.54	0.23	10, 70. 71, 72, 000
HIP028734B . . .	9.59659	0.00005	0.0	Fixed	51.7	0.3	36, 00
HIP028734A . . .	4810.	. . .	0.325	. . .	12.	. . .	37, 00
HIP034608 . . .	113.346	0.006	0.400	0.014	20.75	0.38	13, 00
HIP037629 . . .	19.60447	0.00007	0.0210	0.0069	34.79	0.25	38, 00
. . .	19.60415	0.00008	0.0150	0.0038	34.58	0.13	10, 38, 00
HIP039424 . . .	2437.8	2.9	0.060	0.021	5.19	0.10	39, 00
HIP043109 . . .	5497.3	2.3	0.6558	0.0018	8.05	0.14	40, 41, 00
HIP045527 . . .	922	Fixed	0.293	0.037	9.98	0.35	14, 00
. . .	915.60	0.39	0.233	0.046	9.44	0.40	26, 30, 10, 000
HIP047205 . . .	2834	4	0.322	0.019	6.33	0.15	42, 00
HIP049841 . . .	1585.8	5.6	0.138	0.037	3.74	0.17	43 00
. . .	1607.6	1.4	0.247	0.057	3.98	0.26	26, 10, 000
HIP050801 . . .	230.089	0.039	0.061	0.022	7.43	0.16	15, 00
. . .	230.025	0.018	0.078	0.026	7.67	0.21	15, 000
HIP051233 . . .	14391	Fixed	0.66	Fixed	3.18	0.34	44, 00
. . .	14102	315	0.754	0.051	4.45	0.48	26, 30, 32, 44, 45, 10, 000
HIP052085 . . .	1345.7	5.2	0.237	0.070	4.17	0.31	10, 000
HIP053240 . . .	1166	7	0.375	0.035	4.40	0.21	46, 00
HIP057791 . . .	486.7	1.2	0.309	0.032	13.92	0.43	16, 00
. . .	490.72	0.16	0.329	0.010	14.31	0.34	30, 47, 10, 16, 000
HIP059856 . . .	1314.3	0.4	0.426	0.016	6.54	0.13	48, 00
HIP060170 . . .	5792	85	0.55	0.04	1.90	0.11	49, 00
HIP060351 . . .	396.567	0.047	0.61	0.01	25.1	0.4	17, 00
HIP061724 . . .	972.4	1.4	0.590	0.007	10.46	0.13	18, 00
HIP061910S . . .	44.4137	0.0085	0.25	0.04	25.9	0.9	66,00
. . .	44.4939	0.0009	0.242	0.035	25.73	0.82	66,000
HIP062886 . . .	2914	10	0.67	0.03	5.97	0.57	64, 00
HIP069879 . . .	212.085	0.002	0.574	0.005	20.14	0.17	19, 00
HIP075325 . . .	11.1345	0.0005	0	Fixed	38.6	0.4	8, 00
HIP076425 . . .	5324	19	0.345	0.024	3.86	0.09	50, 00
HIP076566 . . .	14.284	0.011	0.31	0.07	9.92	0.58	11, 00
HIP078259 . . .	9.01490	0.00007	0	Fixed	53.47	0.18	9, 00
HIP078481 . . .	1223.53	1.38	0.219	0.068	3.53	0.21	26, 30, 10, 000
HIP080816 . . .	410.61	0.78	0.545	0.015	12.84	0.29	51, 0
. . .	411.026	0.045	0.546	0.011	13.09	0.23	51, 23, 24, 32, 10, 000
HIP083138 . . .	880.47	0.68	0.119	0.071	3.36	0.21	30, 000
HIP083947 . . .	876.35	0.12	0.625	0.005	4.90	0.04	52, 00

Table 12
(Continued)

Star	P	σ_{P}	e	σ_{e}	K	σ_{K}	Ref.
HIP084402 . . .	2493	11	0.497	0.062	8.54	1.01	10, 68, 69, 000
HIP090135 . . .	2373.8	4.1	0.102	0.036	5.77	0.23	53, 00
. . .	2380.0	2.6	0.114	0.044	5.67	0.26	53, 000
HIP091751 . . .	485.3	0.3	0.209	0.011	9.68	0.12	54, 00
HIP092512 . . .	138.420	0.016	0.114	0.014	23.5	0.3	55, 0
. . .	138.4455	0.0043	0.129	0.019	23.17	0.49	26, 55, 10, 000
HIP092872 . . .	2994	29	0.243	0.026	4.65	0.13	56, 00
HIP093244 . . .	1270.6	1.1	0.272	0.026	5.17	0.13	57, 00
HIP094521 . . .	856	39	0.66	. . .	5.99	0.40	67, 00
HIP095066 . . .	266.544	0.013	0.833	0.002	29.86	0.19	58, 00
HIP103519 . . .	635.1	0.5	0.441	0.023	6.44	0.18	59, 00
HIP104732 . . .	6489	31	0.22	0.03	3.31	0.12	65, 00
HIP112158 . . .	818.0	2.2	0.155	0.011	14.20	0.13	60, 00
. . .	817.464	0.089	0.154	0.013	14.52	0.19	60, 26, 23, 24, 10, 61, 000
HIP116584 . . .	20.5212	0.0003	0.040	0.024	6.64	0.17	12, 00

Notes. Column 2: period P in days, Column 3: uncertainty in the value of the period σ_{P}, Column 4: eccentricity e, Column 5: uncertainty in the value of eccentricity σ_{e}, Column 6: projected orbital velocity of the primary K km s^{-1}, Column 7: uncertainty in the value of K_{A}, denoted by σ_{K}. Column 8: reference.

References. (0) Our solution using the original data, (00) published solution, (000) our solution using the CfA and published data, (1) Pourbaix et al. (2004), (2) De & Udry (1999), (3) Young (1944), (4) Harper (1926), (5) Fekel et al. (1999), (6) Fekel & Eitter (1989), (7) Heard (1940), (8) Fekel et al. (1985), (9) Griffin (1978), (10) Beavers & Eitter (1986), (11) Tokovinin et al. (1998), (12) Walker (1944), (13) Beavers & Salzer (1985), (14) Jones (1928b), (15) Jackson et al. (1957), (16) Ginestet et al. (1985), (17) Abt & Willmarth (1999), (18) Griffin (1981a), (19) Scarfe & Alers (1975), (20) Griffin (1998), (21) Bakos (1976), (22) Lord (1905), (23) Kustner (1908), (24) Lunt (1918), (25) Jones (1928), (26) Campbell & Moore (1928), (27) Tokovinin & Smekhov (2002), (28) Griffin & Herbig (1981), (29) Griffin et al. (1992), (30) Abt (1970), (31) Harper (1935), (32) Harper (1933), (33) Griffin & Gunn (1977), (34) Griffin et al. (1985), (35) Vennes et al. (1998), (36) Griffin & Radford (1976), (37) Ishida (1985), (38) Bopp & Dempsey (1989), (39) Griffin (1982a), (40) Hartkopf et al. (1996). (41) Bakos & Tremko (1987), (42) Griffin (1985), (43) Spencer Jones (1928), (44) Underhill (1963), (45) Abt et al. (1980), (46) Griffin (1980), (47) Snowden & Young (2005), (48) Griffin (1984), (49) Griffin (1991a), (50) Griffin (1991b), (51) Plummer (1908), (52) Griffin (2004), (53) Grobben & Michaelis (1969), (54) Griffin (1982b), (55) Young (1921), (56) Griffin (1981b), (57) Griffin (1982c), (58) Franklin (1952), (59) Radford & Griffin (1975), (60) Crawford (1901), (61) Parsons (1983), (62) Butler (1998), (63) Torres et al. (1997), (64) Griffin et al. (1988), (65) Griffin & Keenan (1992), (66) Sanford & Karr (1942), (67) Setiawan et al. (2004), (68) Andersen (1985), (69) Clark (1989), (70) Andersen et al. (1987), (71) Andersen & Nordström (1983a), (72) Andersen & Nordström (1983b).

Table 13
Published Double-Lined Orbits

Star	P	σ_{P}	e	σ_{e}	K_{A}	σ_{KA}	K_{B}	σ_{KB}	
HIP004463 . . .	115.7140	0.0055	0.0081	0.0054	17.91	0.44	19.85	0.50	1
HIP010280A . . .	14.732	. . .	0.04	. . .	56.5	. . .	57.0	. . .	1
HIP014328 . . .	5329.9	1.7	0.7856	0.0038	13.67	0.22	18.57	0.31	1
HIP016042 . . .	6.4378703	0.0000069	0	Fixed	57.86	0.17	66.98	0.04	1
. . .	6.437920	0.000020	0	Fixed	58.60	0.91	66.92	0.24	1
HIP024608 . . .	104.0240	0.0020	0.0015	0.0011	26.08	0.10	27.44	0.29	1
HIP047508 . . .	14.498080	0.000009	0.000	0.002	54.80	0.08	62.08	0.16	1
HIP057565 . . .	71.69060	0.00040	0	Fixed	30.12	0.07	33.0	1.4	1
. . .	71.69060	0.00058	0.0000	0.0052	29.91	0.34	32.85	0.77	1
HIP061910N . . .	1.4605	. . .	0.09	. . .	88.2	. . .	100	. . .	1
HIP065474 . . .	4.0145	. . .	0.18	. . .	120	. . .	189	. . .	1
HIP066511 . . .	47.9578	0.0022	0.0340	0.0030	31.07	0.10	37.2	0.6	1
HIP076563 . . .	3.273284	0.000073	0	Fixed	86.35	0.49	87.97	0.51	1
HIP084949 . . .	2018.8	0.7	0.6720	0.0020	12.89	0.32	18.32	0.07	1
HIP094013 . . .	28.5903	0.0004	0.010	0.004	40.74	0.16	45.05	0.69	2
HIP096683 . . .	434.169	0.015	0.5420	0.0063	27.45	0.23	28.41	0.30	1
HIP104987 . . .	98.8215	0.0164	0.0044	0.0072	16.06	0.34	18.37	0.72	1
HIP112997 . . .	24.64877	0.00003	0	Fixed	34.29	0.04	62.31	0.06	3

Notes. Column 2: period P in days, Column 3: uncertainty in the value of the period σ_{P}, Column 4: eccentricity e, Column 5: uncertainty in the value of eccentricity σ_{e}, Column 6: projected orbital velocity of the primary K_{A} km s^{-1}, Column 7: uncertainty in the value of K_{A}, denoted by σ_{KA} Column 8: projected orbital velocity of the secondary K_{B} in km s^{-1}, Column 9: uncertainty in the value of K_{B}, denoted by σ_{KB}.

References. (1) Pourbaix et al. (2004), (2) De & Udry (1999), and (3) Marsden et al. (2005) .

Table 14
Single-Lined Primaries with Giants: Physical Parameters

Star	V_{rot}	$\log(L/L_{\odot})$	$\log T_{eff}$	$R/R_{\odot}$	$M_{FA}/M_{\odot}$	$M_{PT}/M_{\odot}$	Note
HIP000443	0.0	1.38	3.669	7.4	1.3	...	...
HIP000626	3.8	1.29	3.684	6.3	1.5	...	...
HIP003092	6.5	1.87	3.635	15.7	1.2	...	...
HIP003675	3.6	1.60	3.682	9.1	1.9	...	...
HIP003693	39.3	1.92	3.662	14.4	1.8	1.4	...
HIP005951	4.5	1.56	3.695	7.9	2.0	...	...
HIP007143	0.0	0.80	3.687	3.5	1.2	...	...
HIP007719	0.0	1.66	3.700	8.9	2.4	...	...
HIP008645	3.2	2.38	3.661	24.5	3.0	3.0	...
HIP008833	0.0	1.65	3.694	9.1	2.5	2.2	...
HIP010366	0.0	1.41	3.684	7.0	1.5	...	...
HIP011840	0.0	1.52	3.665	8.9	1.3	...	...
HIP013531	3.5	2.03	3.677	15.2	2.6	2.2	1
HIP015900	5.9	2.10	3.704	14.6	3.1	3.0	...
HIP020455	5.8	1.82	3.688	11.6	2.5	2.2	...
HIP020885	4.2	1.80	3.695	11.0	2.7	2.5	...
HIP022055	0.0	0.92	3.719	3.5	1.6	...	...
HIP022176	3.7	1.66	3.643	11.7	1.0	...	...
HIP023221	4.3	1.20	3.718	4.8	1.9	...	...
HIP023896	0.0	1.08	3.679	5.0	1.2	...	...
HIP024727	0.0	2.05	3.631	18.8	1.1	...	...
HIP025282	1.1	1.40	3.685	7.0	1.7	...	...
HIP034608	0.0	0.71	3.694	3.1	1.2	...	...
HIP037629	26.2	1.53	3.659	9.3	1.4	...	...
HIP039198	0.0	0.98	3.709	3.9	1.7	...	...
HIP039424	3.9	1.90	3.660	14.5	2.2	1.4	...
HIP040221	0.0	0.71	3.692	3.1	1.1	...	...
HIP041935	3.1	1.34	3.659	7.5	1.0	...	...
HIP043109	7.2	1.68	3.683	9.9	2.0	1.7	1
HIP045527	3.4	1.88	3.649	14.5	1.4	1.0	...
HIP047205	3.0	1.71	3.672	10.8	1.7	1.3	...
HIP049841	2.1	1.66	3.682	10.0	2.2	1.9	...
HIP050801	7.5	3.06	3.590	74.7	...	2.2	...
HIP051233	7.0	1.56	3.699	8.0	2.2	2.2	...
HIP052085	3.5	1.66	3.695	9.1	2.2	2.2	...
HIP053240	0.5	1.31	3.696	6.1	1.8	...	...
HIP057791	1.3	1.58	3.672	9.3	1.5	1.0	...
HIP059856	0.6	2.04	3.652	17.1	1.6	1.2	...
HIP060170	2.9	1.23	3.660	6.5	1.0	...	...
HIP060351	9.0	1.59	3.719	7.5	2.5	...	1
HIP061724	1.5	1.68	3.684	9.9	2.0	1.8	...
HIP062886	4.2	1.97	3.700	13.0	3.0	3.0	...
HIP066511	0.0	1.05	3.684	4.8	1.3	...	...
HIP069879	2.1	1.79	3.670	11.9	1.8	1.4	...
HIP072706	2.9	0.84	3.673	3.9	1.0	...	...
HIP074896	7.7	1.62	3.687	9.0	2.2	2.2	...
HIP075325	37.6	1.08	3.662	5.4	1.0	...	...
HIP076425	1.4	1.57	3.690	8.4	2.2	2.2	...
HIP078481	1.2	1.91	3.679	13.0	2.3	1.9	...
HIP080816	2.8	2.17	3.688	16.9	3.0	3.0	...
HIP083138	4.6	1.60	3.652	10.4	1.2	...	...
HIP083947	4.3	2.01	3.634	18.0	1.2	...	...
HIP084402	3.1	1.62	3.663	10.1	1.4	1.0	...
HIP090135	2.2	1.65	3.688	9.3	2.2	1.8	...
HIP091751	0.0	1.31	3.677	6.6	1.4	...	...
HIP092512	16.5	2.24	3.643	21.8	1.8	1.6	...
HIP092872	0.0	1.70	3.671	10.6	1.8	1.0	...
HIP093244	4.4	1.78	3.671	11.9	2.0	1.4	...
HIP094013	14.1	1.40	3.668	7.7	1.2	...	...
HIP094521	0.0	1.05	3.685	4.8	1.4	...	...
HIP095066	1.2	1.32	3.691	6.3	1.8	...	...
HIP103519	3.3	1.59	3.686	8.9	2.2	...	...
HIP104732	3.6	2.05	3.685	15.2	3.0	3.0	...

Table 14
(Continued)

Star	$V_{\rm rot}$	$\log(L/L_{\odot})$	$\log T_{\rm eff}$	$R/R_{\odot}$	$M_{\rm FA}/M_{\odot}$	$M_{\rm PT}/M_{\odot}$	Note
HIP110900	3.4	0.73	3.691	3.2	1.2	...	...
HIP112158	4.0	2.38	3.682	22.2	3.5	3.5	1
HIP112997	28.1	1.70	3.660	11.5	1.4	...	...
HIP116584	7.3	1.29	3.676	6.3	1.3	...	...

Notes. Column 2: projected rotational velocity $V_{\rm rot} \sin i$ for the primary, km s^{-1}, Column 3: log of the bolometric luminosity of the primary, in solar units $L_{\odot}$, Column 4: $T_{\rm eff}$ is in kelvin, Column 5: radius of the primary, in solar units $R/R_{\odot}$, Column 6: mass of the primary on its "first ascent" in solar masses $M_{\rm FA}/M_{\odot}$, Column 7: mass of the primary if "post-giant tip" in solar masses $M_{\rm PT}/M_{\odot}$, Column 8: 1 stands for star with a composite spectrum due to a hot companion. $T_{\rm eff}$ is calculated using the primary's spectral type. The spectral type is from Parsons & Ake (1998).

Table 15
Double-Lined Systems with Giants: Physical Parameters

Star	$\log T_{\rm A}$ $\log T_{\rm B}$	LightRatio	$\log(L_{\rm A})$ $\log(L_{\rm B})$	$M_{\rm A}$(FA)/M$_{\odot}$ $M_{\rm B}$(FA)/M$_{\odot}$	$M_{\rm A}$(PT)/M$_{\odot}$ $M_{\rm B}$(PT)/M$_{\odot}$	$V_{\rm Arot}$ $V_{\rm Brot}$	$R_{\rm A}/R_{\odot}$ $R_{\rm B}/R_{\odot}$
HIP004463	3.692	0.68	+1.73	2.2	2.2	4.6	9.9
...	3.692	...	+1.57	2.2	2.2	4.7	8.2
HIP004592	3.662	0.16	+1.29	1.1	...	3.6	7.3
...	3.708	...	+0.49	1.1	...	0.0	2.4
HIP10280A	3.693	0.41	+1.79	...	1.6	32.9	4.0
...	3.812	...	+1.00	1.4	...	3.0	1.5
HIP016042	3.662	0.66	+0.67	1.1	...	40.0	3.0
...	3.760	...	+0.16	1.0	...	9.5	1.5
HIP057565	3.685	0.80	+1.63	2.0	2.0	7.3	9.4
...	3.889	...	+1.32	1.8	...	70.0	2.6
HIP078259	3.680	0.25	+0.56	1.0	...	16.0	2.8
...	3.700	...	−0.03	0.8	...	3.7	1.3
HIP096683	3.688	0.77	+1.64	2.0	2.0	4.7	8.9
...	3.688	...	+1.53	2.0	2.0	4.8	7.8
HIP116243	3.710	0.27	+0.88	1.7	...	0.0	3.5
...	3.840	...	+0.50	1.3	...	0.0	2.7

Notes. The mass ratio used for HIP057565 is from Pourbaix (2000); Column 2: $T_{\rm eff}$ is in kelvin, Column 3: ratio of the luminosity of the two components within the wavelength range used by our study, Column 4: log of the bolometric luminosity of the component, in solar units $L_{\odot}$, Column 5: mass of the component, if on its "first ascent," in solar masses $M_{\rm FA}/M_{\odot}$, Column 6: mass of the component, if "post-giant tip," in solar masses $M_{\rm PT}/M_{\odot}$, Column 7: projected rotational velocity $V_{\rm rot} \sin i$ for the component, km s^{-1}, Column 8: radius of the component, in solar units $R/R_{\odot}$.

analysis, also reported in Table 15, and adopting a $B - V$ for the secondary corresponding to its effective temperature) in order to derive an effective temperature and luminosity for the primary from the photometry, and then for the secondary. For FA giants, where the evolutionary stage is unambiguous, the evolutionary tracks then allow an estimate of the mass ratio. In all cases, this mass ratio was consistent with the mass ratio from the orbital solution.

5. EVOLUTION OF ROTATION IN ISOLATED GIANTS

In this section, we look for evidence of stars whose outer layers have been spun up by the ingestion of a planet as the host star evolved up the giant branch. For this experiment, we need a sample of giants where we expect the rotation to be small otherwise.

In the preceding section, we saw that tidal forces can synchronize stellar rotation with orbital motion for giants in binaries with periods less than about 100 days. Thus we invested considerable effort in the identification of spectroscopic binaries with periods less than a few hundred days, so that they could be removed from the sample we want to use to look for evidence of ingested planets. We also needed to eliminate giants that are still rotating rapidly because they have not yet evolved across the transition near spectral type G0 to G3 for luminosity classes IV and III (Gray 1989), where there is a strong braking mechanism that curtails stellar rotation rather abruptly as stars evolve to cooler temperatures.

The transition from rapid rotation to slow rotation is illustrated by the isolated giants in our sample, namely those giants where we are confident that tidal forces are not important, either because there is no sign of velocity variation due to an orbiting companion, or the orbital period must be too long for tidal interactions to be significant even if there is a stellar companion. In Figure 11, we plot our isolated giants on the M_V versus $B - V$ color–magnitude diagram, using color-coded symbols to show the line broadening of each star. The hotter giants on the left-hand side of the diagram are dominated by rapidly-rotating stars plotted as blue diamonds. The cooler giants on the right-hand side of the diagram rotate more slowly. The less luminous giants on the cool side are dominated by slowly-rotating stars plotted in gray and yellow. Moving up to more luminous giants, the preponderance of red symbols suggests that rotation tends to be faster for giants on the horizontal branch than for stars on the first ascent of the giant branch. The transition from rapid to

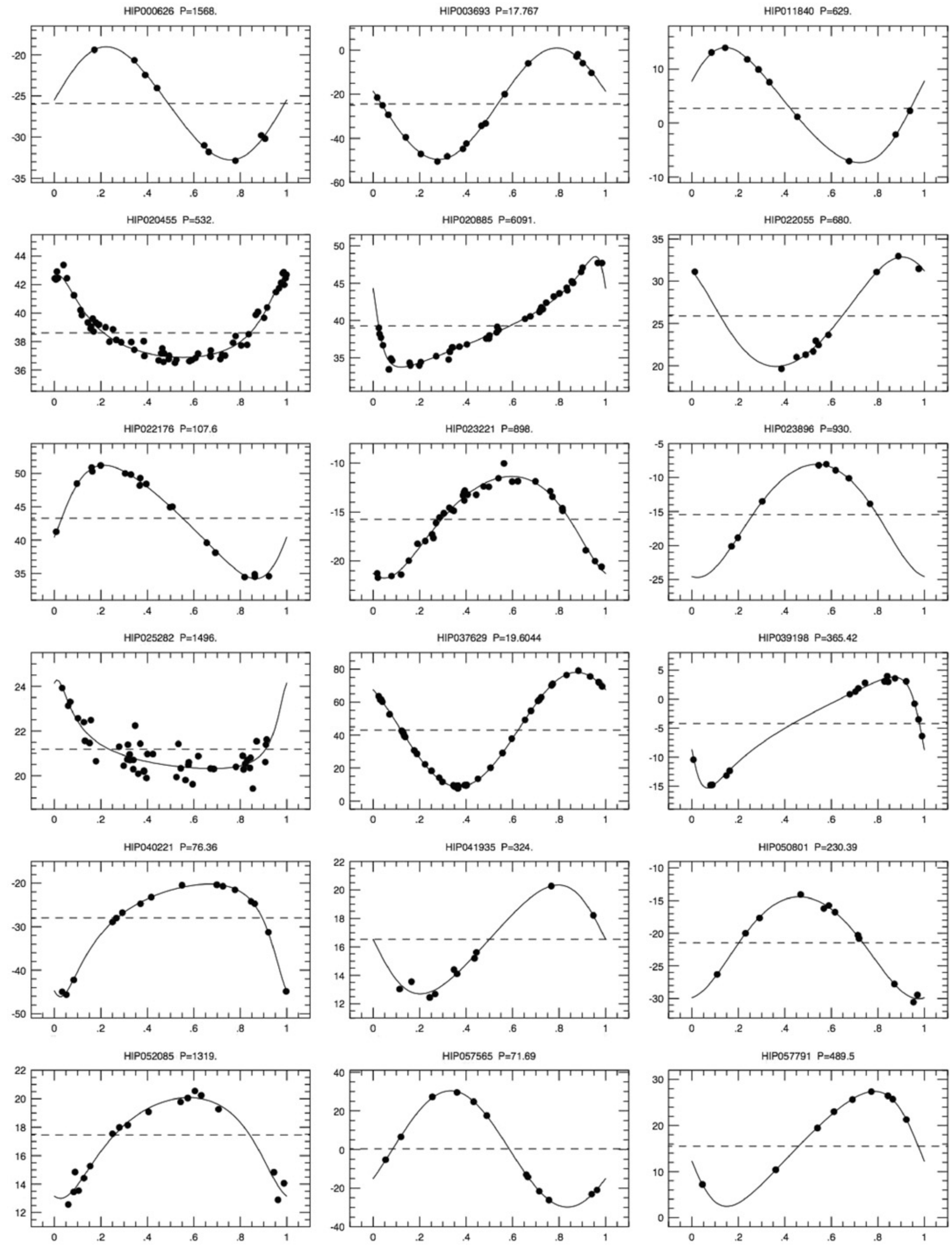

Figure 6. Velocity curves for the CfA single-lined orbital solutions. The individual velocities for primaries are plotted as filled circles. The vertical axes are velocity in km s^{-1}, the horizontal axes are orbital phase.

slow rotation occurs at roughly $B - V = 0.8$, or spectral type G2 III.

Of course, we selected our sample of giants from the Hipparcos Catalogue so that we could use the observed parallaxes and photometry to derive luminosities and effective temperatures. This allows us to plot our isolated giants together with evolutionary tracks on a $\log(L/L_\odot)$ versus $T_{\rm eff}$ diagram, shown in Figure 12. In this diagram, the transition from rapid to slow rotation is marked by a rich population of slowly-rotating giants cooler than about $\log T_{\rm eff} = 3.7$, or $T_{\rm eff} = 5000$ K. It is the sample of isolated giants at evolutionary stages cooler than this transition that we use to search for evidence of ingested planets. To guide our discussion of evolutionary stages, we once again plot the Girardi et al. (2000) evolutionary tracks for [Fe/H] $= -0.2$ in Figure 12, exactly as we did in Figure 8. HIP053449, an AGB giant of spectral type M5.5 III that has already completed its third dredge up (Lebzelter & Hron 2003) was not included in Figure 12, since its surface temperature determination using colors was not possible.

Some interesting patterns at relatively slow rotations near our detection threshold are apparent in Figure 12. Stars with

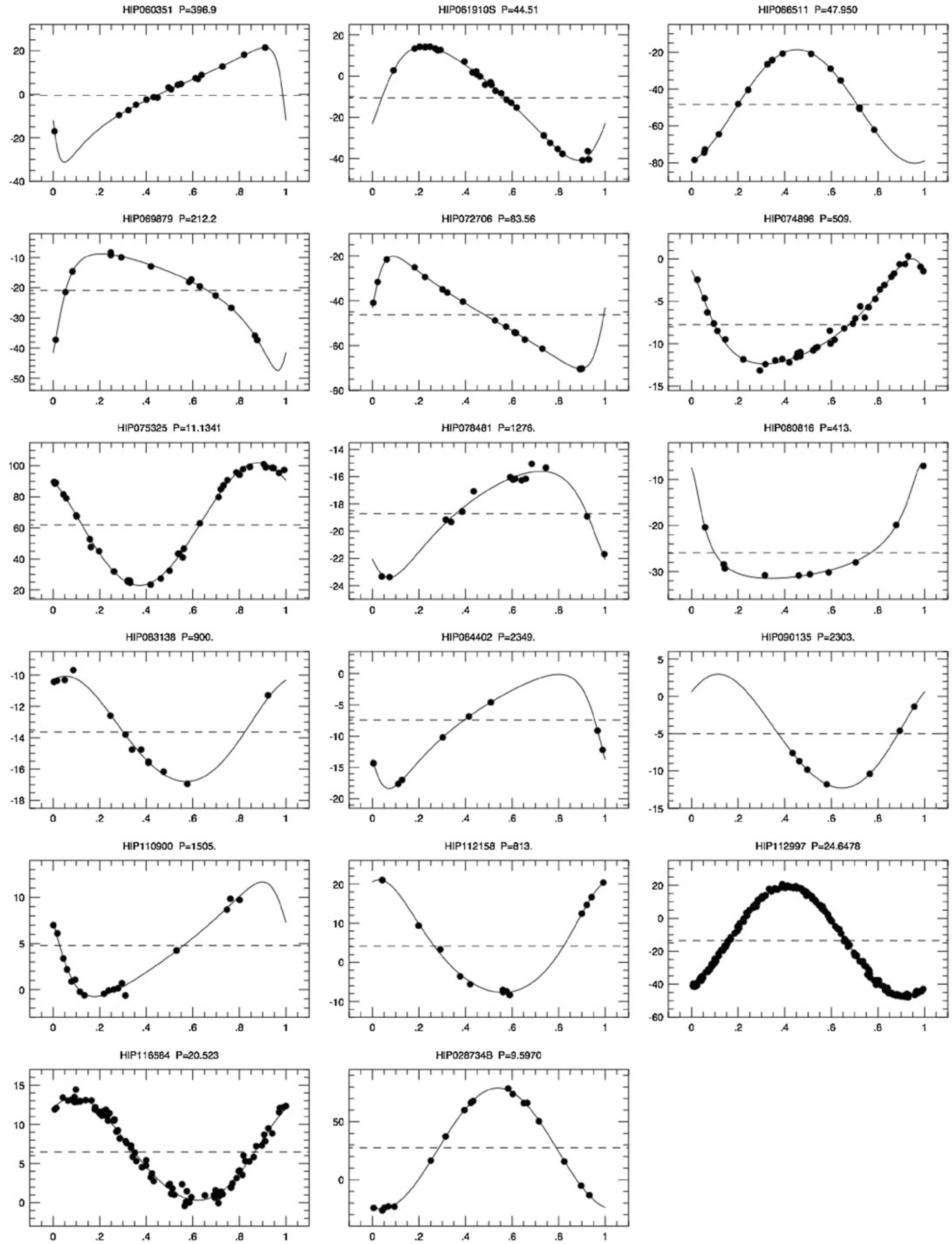

Figure 6. (Continued).

masses in the range 1.0–1.4 $M_{\odot}$ start their climb up the giant branch with little or no detectable rotation; most of these stars show less than 2 km s^{-1} of rotation, while only a few are in the range 2–4 km s^{-1}. When the first dredge-up line is crossed (Girardi et al. 2000), several stars that are unambiguously on the first ascent of the giant branch show excess rotation of up to 6.3 km s^{-1}. An expanded plot of this region of the diagram is shown in Figure 13; the locus of first dredge-up is plotted for [Fe/H] = 0.0 (dashed red line) and [Fe/H] = −0.2 (dashed blue line). If this transition is real, it suggests that the first dredge-up transfers significant angular momentum from a spinning core to the observable outer layers. Our determinations of rotational velocities for stars near first dredge-up should be checked using a Fourier analysis of spectra with higher signal-to-noise ratios and better spectral resolution, to make sure that the macroturbulence is being handled correctly and that detailed abundance analyses show evidence of elements and isotopes brought to the observable surface by the dredge-up. If such investigations confirm that the first dredge-up corresponds to increased surface rotation, it would support the idea that the

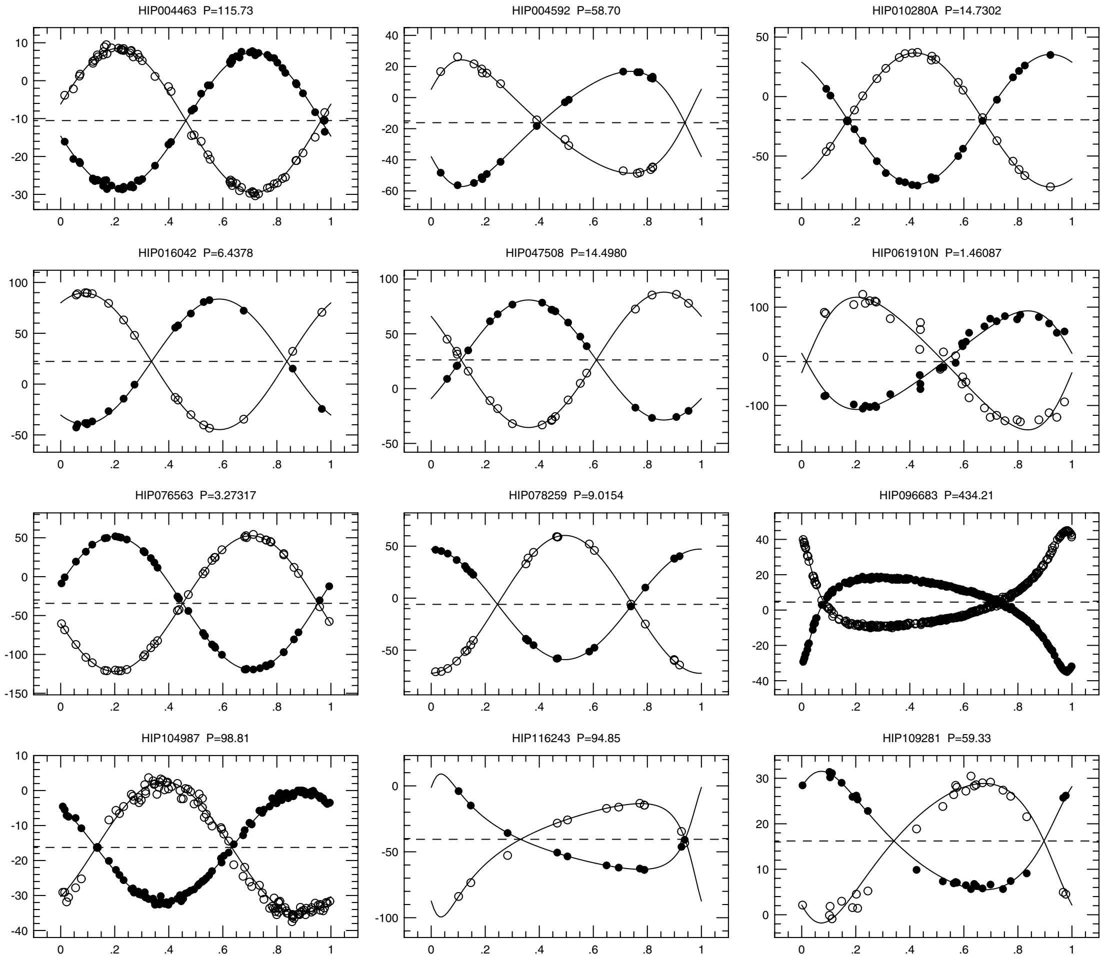

Figure 7. Velocity curves for the CfA double-lined orbital solutions. The individual velocities for primaries are plotted as filled circles, the secondaries as open circles. The vertical axes are velocity in km s^{-1} the horizontal axes are orbital phase.

stellar cores are rotating rapidly. The idea that the cores of solar-mass stars spin rapidly is controversial (cf. Demarque et al. 2001; Thompson et al. 2003).

When we move up from the region below the red clump, where stars are unambiguously on the first ascent of the giant branch, and into the core helium burning region of the HR diagram, where the post-tip evolutionary tracks overlap the first-ascent tracks, we note that several of the giants show hints of modest amounts of excess rotation, with values up to 5.3 km s^{-1} (and two outliers show even faster rotation). Although we cannot tell whether stars in this ambiguous region are first ascent or post-tip, we can show that the velocity distributions are statistically different in the two highlighted regions: one region for unambiguous first-ascent stars and the other for ambiguous stars where the evolutionary tracks overlap. We performed a Kolmogorov–Smirnov (K–S) test on two groups of stars. One group comprised stars with $3.665 < \log T_{\mathrm{eff}} < 3.705$ and $1.20 < \log(L/L_{\odot}) < 1.53$, below the HB, while the other comprised stars with $3.665 < \log T_{\mathrm{eff}} < 3.705$ and $1.54 < \log(L/L_{\odot}) < 1.88$, at the approximate location of the HB (see Figure 13). Figures 14 and 15 are histograms of the two distributions, displaying the number of stars as a function of the observed $V_{\mathrm{rot}} \sin i$. The difference between the two distributions is significant to $p < 10^{-3}$. We then repeated the K–S test but using stars in a group of first ascent giants to the right of the dredge-up line in place of the HB stars. This third group of stars is within the region with $3.650 < \log T_{\mathrm{eff}} < 3.665$ and $1.20 < \log(L/L_{\odot}) < 1.80$, as displayed in Figure 13. The corresponding histogram is Figure 16. Once again, the two distributions are found to be significantly different, with $p < 10^{-3}$.

Assuming it is real, what could be the source of this excess rotation for stars near the red clump? Is this rotation related to the mechanism involved near the first dredge-up line? Alternatively, could this modest excess rotation be the net result of planet ingestion near the red giant tip, as modified by subsequent evolution and loss of mass and angular momentum? If ingested planets are the source of excess rotation, then we might expect that some stars near the red giant tip should show more rotation than others, depending on the mass of the planet and the size of the orbit, and therefore the amount of angular momentum deposited. We do see luminous giants with more line broadening, but we are cautious about assigning this to excess rotation for two reasons. First, we are unsure of the macroturbulence corrections for the most luminous stars. In particular, we note that our synthetic spectra do not match the observed spectra as well for the reddest and most luminous stars as they do for less extreme giants. Second, we note that we do not see as much excess line broadening for the most luminous stars in our sample in contrast to the result found by Carney

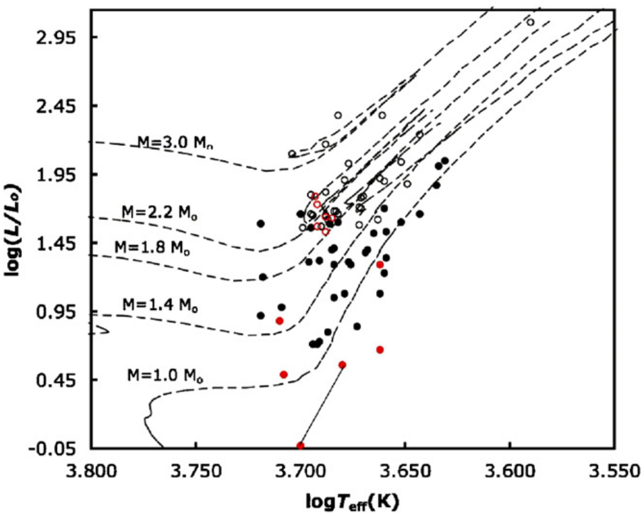

Figure 8. Distribution in $\log(L/L_\odot)$ versus $\log T_{\rm eff}$ for 67 giants in single-lined binaries and 12 giants in eight double-lined binaries with orbital solutions. The dashed lines represent the Girardi et al. (2000) evolutionary tracks for masses $M = 1.0, 1.2, 1.4, 1.8, 2.2, 3.0\ M_\odot$ and metallicity [Fe/H] $= -0.2$. Black stands for single-lined binaries, red for the giant component of double-lined binaries. Filled circles represent stars unambiguously on their first ascent to the tip of the red giant branch, while open circles represent stars that could be either in their first ascent to the red giant tip or already in the HB/AGB evolutionary phase. The bar links the primary and the secondary of HIP 78259. HIP 50801, a star unambiguously in its AGB phase, is also represented by an open circle.

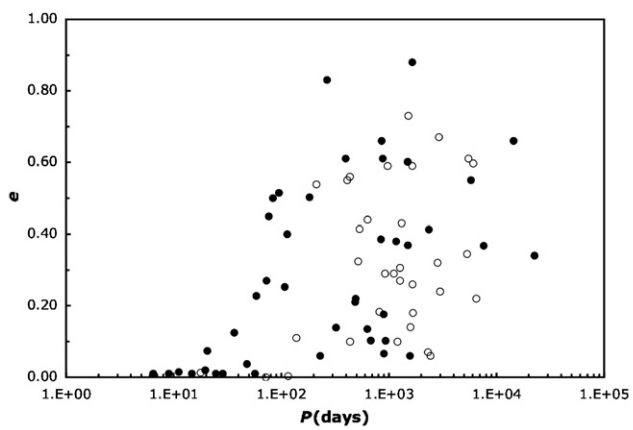

Figure 9. Eccentricity versus orbital period for 75 binary systems. Filled circles stand for the subgroup unambiguously on the first ascent to the red giant tip. Open circles stand for stars whose evolutionary status is ambiguous. Binaries in the latter subgroup may be either on their first ascent or already in their HB or AGB evolutionary phase. HIP 50801, a star unambiguously in its AGB phase, is also represented by an open circle.

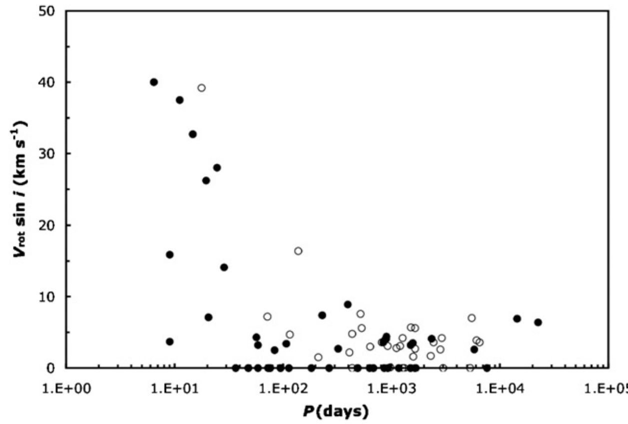

Figure 10. $V_{\rm rot} \sin i$ versus orbital period P for 79 giants in 75 binary systems. Filled circles stand for the subgroup unambiguously on the first ascent to the red giant tip. Open circles stand for stars whose evolutionary status is ambiguous. Binaries in the latter subgroup may either be on their first ascent or already in their HB or AGB evolutionary phase. HIP 50801, a star unambiguously in its AGB phase, is also represented by an open circle.

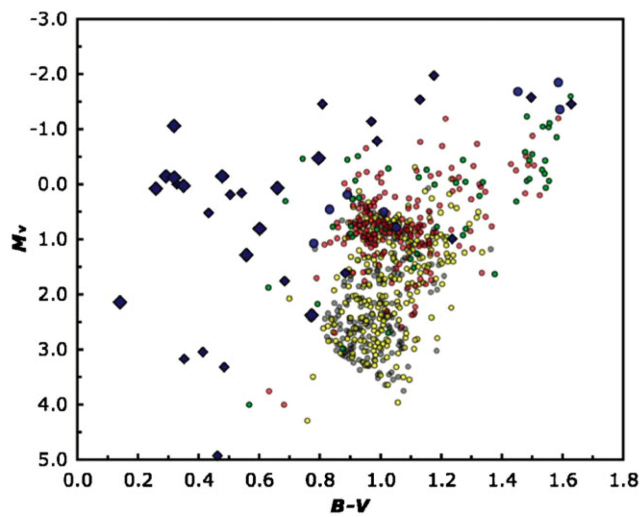

Figure 11. Distribution in M_V versus $B - V$ of all single stars and wide binaries in our sample. Gray circles correspond to line broadening $V_{\rm br} < 2$ km s^{-1}, yellow to 2 to 4 km s^{-1}, red to 4 to 6 km s^{-1}, green to 6 to 8 km s^{-1}, blue to 8 to 10 km s^{-1}, small diamonds 10 to 30 km s^{-1}, and big diamonds to $V_{\rm br} >$ 30 km s^{-1}. Stars in the HB display moderate broadening, as do several stars above that region. Most stars to the left of the HB have large line broadening, as is expected, corresponding to rapid rotation. For these stars "rotational braking" (Gray 1989) has not yet occurred.

et al. (2003) for a metal-poor sample of red giants. It is not clear whether this difference is real or a result of some systematic effect. For example, the Carney et al. metal-poor sample contains more stars that are extremely luminous and red. This is a natural consequence of that fact that our sample of solar-neighborhood stars was selected to lie closer to the Sun than 100 pc and thus contains almost no examples of stars that are intrinsically rare. Also, the luminous metal-poor stars are bluer than the corresponding giants in our solar-neighborhood sample, and thus may not have undergone as much rotational braking. The transition from rapid to slow rotators for supergiants is less well defined than for clump giants, as noted by Gray & Toner (1986, 1987).

In our sample of isolated giants, we found only four outliers that have excess rotation. One of these (HIP 103144) has $V_{\rm rot} \sin i = 76.1$ km s^{-1} and has been classified as an FK Comae star (Bopp & Stencil 1981). The source of the very rapid rotation of FK Comae stars is not well understood. One possibility is common-envelope evolution with a substellar companion, but only if the mass of the companion is less than about 20 $M_{\rm J}$ (Livio & Soker 1984). For more massive companions, mass transfer from the evolving giant onto the companion may save it from a common-envelope death spiral.

A second outlier (HIP 35253), with $V_{\rm rot} \sin i = 9.9$ km s^{-1}, is located below the red clump and presumably is on its first ascent of the giant branch. Its rotation rate is 5.8 km s^{-1} faster than all the other stars of similar mass and evolutionary stage. HIP 35253 is the outlier in Figure 14. The Hipparcos Catalogue reports that HIP 35253 has a visual companion with a separation of 172 ± 4 mas and 0.7 mag fainter, corresponding to a projected

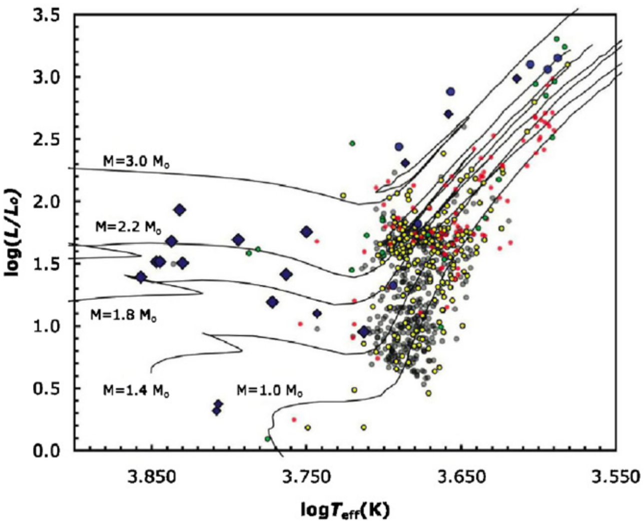

Figure 12. Distribution in $\log(L/L_{\odot})$ versus $\log T_{\rm eff}$ of our isolated giants, with evolutionary tracks from Girardi et al. (2000) for mass $M = 1.0, 1.4, 1.8, 2.2, 3.0\ M_{\odot}$ and metallicity [Fe/H] $= -0.2$. In most of the region below the HB, stars display very little, or no rotation. Gray circles correspond to $V_{\rm rot} \sin i < 2$ km s^{-1}, yellow to 2 to 4 km s^{-1}, red to 4 to 6 km s^{-1}, green to 6 to 8 km s^{-1}, blue to 8 to 10 km s^{-1}, small diamonds 10 to 30 km s^{-1}, and big diamonds to $V_{\rm rot} > 30$ km s^{-1}. Stars in the HB region display moderate rotation, as do several stars above that region. Many stars to the left of the red giant branch in the diagram are still rapid rotators, as is expected, since for these stars "rotational braking" (Gray 1989) has not yet occurred.

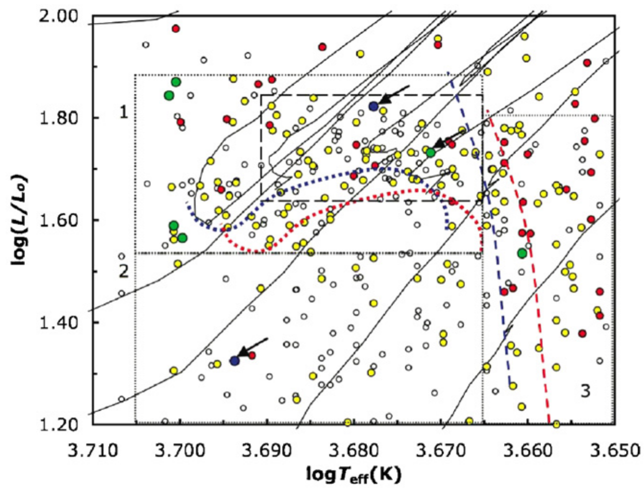

Figure 13. Enlargement of Figure 12, displaying the region around the HB. The position of the moderate rotators in the clump matches very closely the position of stars in the HB according to the evolutionary tracks for various masses and solar metallicity (Girardi et al. 2000). Open circles stand for $V_{\rm rot} \sin i < 2$ km s^{-1}, yellow for 2 to 4 km s^{-1}, red for 4 to 6 km s^{-1}, green for 6 to 8 km s^{-1}, and blue $V_{\rm rot} \sin i > 8$ km s^{-1}. A number of moderate rotators can be seen to the right of the line of first dredge-up, denoted by the red and blue dashed lines, for [Fe/H] $= 0.0$ and [Fe/H] $= -0.2$, respectively. This result suggests that there is an exchange of angular momentum with a rapidly spinning core at the time of first dredge-up. The red and blue dotted lines denote the zero-age HB for the same metallicities. The arrows denote the three stars whose rotation rate is unusually high, and may require some additional spinning-up mechanism, such as planet ingestion. We used stars in the highlighted regions to perform a statistical test, showing that the two subsamples belong to different rotational velocity distributions. We infer that HB branch stars rotate moderately faster than stars with similar physical parameters on their first ascent. Dotted lines delimit the three regions of the diagram that we used for our statistical analysis (see text). The region delimited by the black dashed line includes a subsample of stars in close proximity of the two rapidly rotating clump giants.

separation of 15.6 AU. The CfA velocities show a hint of acceleration over the 3 years of coverage, which could easily be the result of orbital motion around the visual companion. The velocities show no evidence for short-period variations, so excess rotation due to tidal forces from a nearby stellar companion in a hierarchical triple system appears to be ruled out.

The final two outliers are both located in the red clump, and thus have ambiguous evolutionary histories. In Figure 17, they lie more than 2.4 km s^{-1} beyond all the other stars in the same region of the H–R diagram, with rotation rates of 8.4 and 7.7 km s^{-1} for HIP 36896 and HIP 81437, respectively. HIP 36896 also has a visual companion according to the Hipparcos Catalogue, at a separation of 198 ± 4 mas and 0.4 mag fainter. In this case, there is a combined visual and speckle orbit (Hartkopf et al. 1989) with $P = 213.1 \pm 5.8$ years and $e = 0.693 \pm 0.007$. For this star, the CfA velocities also show a hint of acceleration over the 3 years of coverage, but no sign of short-period velocity variations that might be attributed to a close companion. HIP 81437 clearly shows slowly-changing velocity variations over the 4 years of CfA observations, without covering a full orbital period. Harris & McClure (1983) published 17 velocities for HIP 81437, obtained over a period of 3 years starting in 1979, and they also show a slow velocity variation. Together, the two sets of velocities suggest that the orbital period may be about 9 years with only modest eccentricity. Adding in a few earlier velocities from the Lick, Mount Wilson, and Dominion Astrophysical Observatories did not lead to an unambiguous orbit. Again, there is no sign of short-period velocity variations.

A possible explanation for the anomalous rotation of these stars is ingestion of planets. What minimum mass would a planet have to have in order to spin up these stars to the observed rotation rate? Conservation of angular momentum at the time of

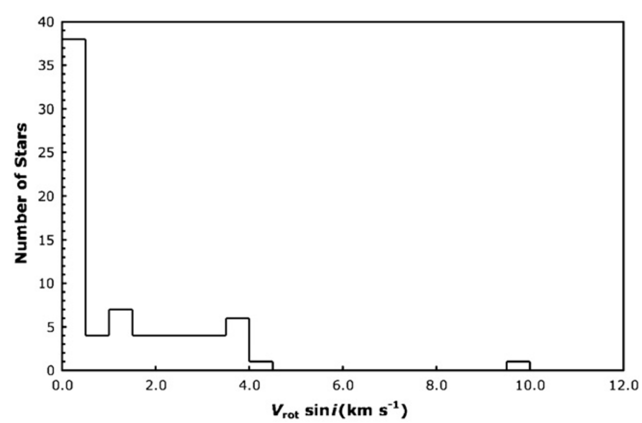

Figure 14. Histogram showing the distribution of isolated giants as a function of rotational velocity in region 2 of Figure 13. Few stars have any measurable rotation. There is one clear outlier, HIP 35253, whose $V_{\rm rot} \sin i = 9.9$ km s^{-1}. This is a candidate for the planet ingestion mechanism discussed in the text.

ingestion leads to the following expression:

$$\begin{aligned}\Delta V_{\rm rot} &= \frac{m_{\rm p}}{M r_{\rm g}^2}\sqrt{\frac{GM}{R}} \\ &= 4.4\left[\frac{M}{M_{\odot}}\right]^{-1/2}\left[\frac{R}{R_{\odot}}\right]^{-1/2}\left[\frac{m_{\rm p}}{M_{\rm J}}\right]\left[\frac{10^{-1}}{r_{\rm g}^2}\right] \text{km s}^{-1}\end{aligned} \tag{3}$$

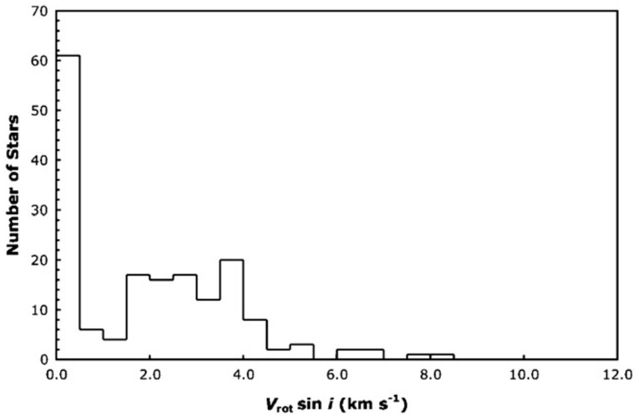

Figure 15. Histogram showing the distribution of isolated giants as a function of rotational velocity in region 1 of Figure 12. This distribution is statistically different from that of region 2, as shown by a K–S test that we performed on the two samples. Several stars have 2 km s^{-1} < $V_{\rm rot} \sin i$ < 4 km s^{-1}, and six stars have $V_{\rm rot} \sin i > 6$ km s^{-1}. Four of these more rapid rotators are located on the far left of region 1, while two are in the middle of the HB.

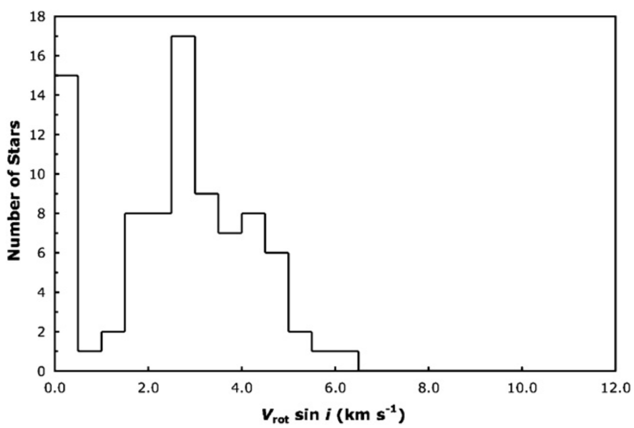

Figure 16. Histogram showing the distribution of isolated giants as a function of rotational velocity in region 3 of Figure 12. This distribution is statistically different from that of region 2, as shown by a K–S test that we performed on the two samples. A possible explanation of the difference in the two samples, both containing stars on their first ascent to the giant branch tip, is that as stars undergo the first dredge-up their envelope exchanges angular momentum with a rapidly rotating core.

for the difference between the initial rotational speed of the star and its value immediately after ingestion. In this simplified calculation, we assumed that the angular momentum of the planet of mass m_p is imparted to an envelope of angular momentum $J = I\Delta V_{\rm rot}/R$, where the moment of inertia is $I = r_g^2 MR^2$ and we chose $r_g^2 = 10^{-1}$ for simplicity (Siess & Livio 1999a). Note that, even though the angular momentum contributed by a planet scales like $(R/R_\odot)^{1/2}$, the resulting $\Delta V_{\rm rot} \propto (R/R_\odot)^{-1/2}$ because of the linear dependence of the stellar angular momentum on the stellar radius.

Let us assume that all four of these rapidly rotating stars are on their first ascent of the giant branch. For the minimum amount that the rotation rate has increased for each star, we take $\Delta V_{\rm rot}$ to be the difference between the measured value of $V_{\rm rot} \sin i$ minus the value for the fastest nonoutlier with comparable physical properties. We find minimum ingested planet masses of $m_p \gtrsim 2.8 M_{\rm J}$ for HIP 36896, $m_p \gtrsim 2.4 M_{\rm J}$ for HIP 81437, $m_p \gtrsim 4.5 M_{\rm J}$ for HIP 35253, and $m_p \gtrsim 40\ M_{\rm J}$ for HIP 103144.

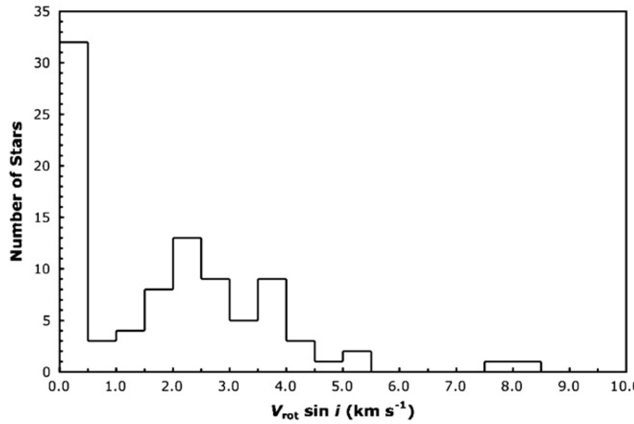

Figure 17. Histogram showing the distribution of isolated giants as a function of rotational velocity in the dashed bounded area within region 1 of Figure 13. This sample contains stars in close proximity to the two clump outliers HIP 36896, with $V_{\rm rot} \sin i = 7.7$ km s^{-1} and HIP 81437, with $V_{\rm rot} \sin i = 8.4$ km s^{-1}. As in the case of HIP 35253, one may explain the unusual rotational velocity of these two stars by invoking planet ingestion.

There are two other effects that ensure that these estimates are lower limits for first ascent stars, namely there may have been further evolution to larger size after the ingestion event and stellar winds may have carried some of the angular momentum away from the envelope.

If the two clump stars are in their HB phase instead of first ascent, they would have reached a maximum radius $R \simeq 120\ R_\odot$ at the red giant tip. A planet ingested during the final stage of the ascent to the giant tip could impart a large amount of angular momentum to the star, proportional to the square root of the semimajor axis of its orbit. For the HB case, we get $m_p \gtrsim 1\ M_{\rm J}$ for both HIP 36896 and HIP 81437.

In summary, the ingestion of a planet of even a few Jupiter masses could provide the observed excess rotation for first ascent giants, and a mass close to Jupiter's would work for post-tip giants. However, more massive ingested planets would be required if mass loss after the tip carried away significant angular momentum, or if stellar winds were important.

6. SUMMARY

We report new rotational and radial velocities for 761 giants chosen from the Hipparcos Catalogue to lie within 100 pc of the sun. The velocities are based on spectra obtained with the CfA Digital Speedometers. We present new orbital solutions for 47 binaries, 13 of which are without a previously published orbital solution. We also combine new data with old measurements to update 23 orbits, and we use published data but modern software to update another four orbits. For the 75 binary systems with giants and with orbital solutions that we analyzed, all of orbits with periods shorter than 20 days have been circularized, while about half the orbits with periods in the range 20–100 days still show significant eccentricity.

We derived effective temperatures, luminosities, and radii using published photometry combined with the Hipparcos distances. We investigated macroturbulence as a function of effective temperature and luminosity using stars with published values based on spectroscopic studies at high spectral resolution and with a high signal-to-noise ratio. We then corrected the spectral line broadening measured with the CfA Digital Speedometers to remove the effects of macroturbulence statistically as a function of effective temperature and luminosity. To look for patterns in rotational velocity as a function of evolutionary stage, we identified a subsample of isolated giants where the stellar rotation should not have been affected by tidal interactions with a stellar companion. We confirm the well-known result that giants hotter than about spectral type G0 to G3 rotate rapidly, while our rotational velocities for most of the cooler giants are less than 2 km s^{-1}.

Several giants that are just past the first dredge-up line, in a part of the luminosity versus effective temperature diagram where they must be on the first ascent of the giant branch, show rotational velocities that are just a few km s^{-1} higher. Perhaps this excess rotation is the result of transfer of angular momentum from spinning stellar cores to the observable surface layers. Another pattern is that giants in the red clump tend to exhibit more rapid rotation than their progenitors on the first ascent, again by just a few km s^{-1}.

Three of our isolated giants have $V_{\rm rot} \sin i$ values in the range 7.7–9.9 km s^{-1} and are outliers in the distribution of rotational velocities. Two of these giants fall in the red clump, while one is clearly on the first ascent of the giant branch. All three are members of long-period binaries with separations that are too large for tidal forces to be important now. We conclude that the excess rotation of these three giants could be the result of ingestion of a giant planet or brown dwarf.

We thank Bob Davis for maintaining our radial-velocity data base and Joe Zajac and Joe Caruso for obtaining many of the observations at the Oak Ridge Observatory. We also thank Bruce Carney and Dimitar Sasselov for their comments on the paper and John Laird, Guillermo Torres, Tsevi Mazeh, and Sören Meibom for useful discussions. This publication makes use of data products from the Two Micron All Sky Survey, which is a joint project of the University of Massachusetts and the Infrared Processing and Analysis Center/California Institute of Technology, funded by the National Aeronautics and Space Administration and the National Science Foundation. This research has made use of the SIMBAD database, operated at CDS, Strasbourg, France.

REFERENCES

Abt, H. A. 1970, ApJS, 19, 387
Abt, H. A., Levy, S. G., & Sanwal, N. B. 1980, ApJS, 43, 549
Abt, H. A., & Willmarth, D. W. 1999, ApJ, 521, 682
Allende Prieto, C., & Lambert, D. L. 1999, A&A, 352, 555
Andersen, J. 1985, A&AS, 59, 15
Andersen, J., & Nordström, B. 1983a, A&AS, 53, 287
Andersen, J., & Nordström, B. 1983b, A&A, 122, 23
Andersen, J., Nordström, B., & Jensen, K. S. 1987, A&AS, 68, 347
Bakos, G. A. 1976, J. RAS. Can., 70, 23
Bakos, G. A., & Tremko, J. 1987, Contr. Astron. Obs. Skalnate Pleso, 16, 17
Barnes, S. A. 2000, ApJ, 586, 464
Beavers, W. I., & Eitter, J. J. 1986, ApJS, 62, 147
Beavers, W. I., & Salzer, J. J. 1985, PASP, 97, 355
Bopp, B. W., & Dempsey, R. C. 1989, PASP, 101, 516
Bopp, B. W., & Stencil, R. E. 1981, ApJ, 247, L131
Butler, R. P. 1998, ApJ, 494, 342
Campbell, W. W., & Moore, J. H. 1928, Publ. Lick Obs., 494, 16
Carney, B. W., Latham, D. W., Stefanik, R. P., Laird, J. B., & Morse, J. A. 2003, AJ, 125, 293
Clark, M. 1989, IAU Inform. Bull. Variable Stars, 125, 3407
Crawford, R. T. 1901, ApJ, 14, 203
Demarque, P. 2001, in ASP Conf. Ser. 223, 11th Cambridge Workshop on Cool Stars, Stellar Systems and the Sun, ed. R. J. Garcia, R. Rebolo Lopez, & M. R. Zapaterio Osorio (San Francisco, CA: ASP) 179
De Medeiros, J. R., Da Rocha, C., & Mayor, M. 1996, A&A, 314, 499
De Medeiros, J. R., Da Silva, J. R. P., & Maia, M. R. G. 2002, ApJ, 578, 943
De Medeiros, J. R., do Nascimento, J. D., Sankarankutty Jr., S., Costa, J. M., & Maia, M. R. G. 2000, A&A, 363, 239
De Medeiros, S., & Mayor, M. 1999, A&AS, 139, 433
De, Medeiros, & Udry, S. 1999, A&A, 346, 532
De Medeiros, J. R., Udry, S., & Mayor, M. 2004, A&A, 427, 313
Do Nascimento, J. D., Canto Martins Jr., B. L., Melo, C. H. F., Porto de Mello, G., & De Medeiros, J. R. 2003, A&A, 405, 723
Duquennoy, A., & Mayor, M. 1991, A&A, 248, 485
ESA 1997 The Hipparcos and Tycho Catalogues, ESA SP-1200
Fekel, F. C. 1997, PASP, 109, 514
Fekel, F. C., & Eitter, J. J. 1989, AJ, 97, 1139
Fekel, F. C., Hall, D. S., Africano, J. L., Gillies, K., Quigley, R., & Fried, R. E. 1985, AJ, 90, 2581
Fekel, F. C., Strassmeier, K. G., Weber, M., & Washuettl, A. 1999, A&AS, 137, 369
Franklin, K. 1952, ApJ, 116, 383
Ginestet, N., Carquillat, J. M., Pédoussaut, A., & Nadal, R. 1985, A&A, 144, 403
Girardi, L., Bressan, A., Chiosi, C., Bertelli, G., & Nasi, E. 2000, A&AS, 141, 371
Gray, D. F. 1981, ApJ, 251, 155
Gray, D. F. 1989, ApJ, 347, 1021
Gray, D. F. 1992, in The Observation and Analysis of Stellar Photospheres, (2nd ed.; Cambridge: Cambridge Univ. Press)
Gray, D. F., & Nagar, P. 1985, ApJ, 298, 756
Gray, D. F., & Toner, C. G. 1986, ApJ, 310, 277
Gray, D. F., & Toner, C. G. 1987, ApJ, 322, 360
Griffin, R. F. 1978, Observatory, 98, 257
Griffin, R. F. 1980, Observatory, 100, 161
Griffin, R. F. 1981a, J. Astrophys. Astron., 2, 115
Griffin, R. F. 1981b, Observatory, 101, 208
Griffin, R. F. 1982a, MNRAS, 200, 1161
Griffin, R. F. 1982b, Observatory, 102, 27
Griffin, R. F. 1982c, Observatory, 102, 82
Griffin, R. F. 1984, J. Astrophys. Astron., 5, 181
Griffin, R. F. 1985, Observatory, 105, 7
Griffin, R. F. 1991a, J. Astrophys. Astron., 12, 39
Griffin, R. F. 1991b, Observatory, 111, 29
Griffin, R. F. 1998, Observatory, 118, 158
Griffin, R. F. 2004, Observatory, 124, 294
Griffin, R. F., Beavers, W. I., & Eitter, J. J. 1988, PASP, 100, 358
Griffin, R. F., Griffin, R. E. M., Gunn, J. E., & Zimmerman, B. A. 1985, AJ, 90, 609
Griffin, R. F., & Gunn, J. E. 1977, AJ, 82, 176
Griffin, R. F., & Herbig, G. H. 1981, MNRAS, 196, 33
Griffin, R. F., & Keenan, P. C. 1992, Observatory, 112, 168
Griffin, R. F., & Radford, G. A. 1976, Observatory, 96, 188
Griffin, R. E. M., Schroder, K. P., Misch, A., & Griffin, R. F. 1992, A&A, 254, 289
Grobben, J., & Michaelis, R. P. 1969, Ricerche Astron., 8, 33
Harper, E. E. 1926, Publ. Dom. Astrophys. Obs., 3, 341
Harper, E. E. 1933, Publ. Dom. Astrophys. Obs., 6, 149
Harper, E. E. 1935, Publ. Dom. Astrophys. Obs., 6, 208
Harris, H. C., & McClure, R. D. 1983, ApJ, 265, 77
Hartkopf, W. L., Mason, B. D., & McAlister, H. A. 1996, AJ, 111, 370
Hartkopf, W. I., McAlister, H. A., & Franz, O. G. 1989, AJ, 98, 1014
Heard, J. F. 1940, Publ. David Dunlap Obs., 1, 194
Ishida, G. 1985, Ap&SS, 110, 161
Jackson, E. S., Shane, W. W., & Lynds, B. T. 1957, ApJ, 125, 712
Jones, H. 1928a, Cape Ann., 10, 40
Jones, H. 1928b, Cape Ann., 10, 49
Kurucz, R. L. 1992, in The Stellar Populations of Galaxies, IAU Symp. No. 149, ed. B. Barbuy, & A. Renzini (Dordrecht: Kluwer) 225
Kurtz, M. J., & Mink, D. J. 1998, PASP, 110, 934
Kustner, F. 1908, ApJ, 27, 301
Latham, D. W. 1992, in IAU Coll. 135, Complementary Approaches to Double and Multiple Star Research, ASP Conf. Ser. 32, ed. H. A. McAlister, & W. I. Hartkopf (San Francisco, CA: ASP) 110
Latham, D. W., Stefanik, R. P., Torres, G., Davis, R. J., Mazeh, T., Carney, B. W., Laird, J. B., & Morse, J. A. 2002, AJ, 124, 1144
Lebzelter, T., & Hron, J. 2003, A&A, 411, 533
Livio, M. 1982, A&A, 112, 190
Livio, M., & Soker, N. 1984, MNRAS, 208, 763
Lord, H. C. 1905, ApJ, 21, 297L
Lunt, J. 1918, ApJ, 48, 261
Marsden, S. C., et al. 2005, ApJ, 634, L173

Mathieu, R. D., Duquennoy, A., Latham, D. W., Mayor, M., Mazeh, T., & Mermilliod, J.-C. 1992, in Binaries as Tracers of Stellar Formation, ed. A. Duquennoy, & M. Mayor (Cambridge: Cambridge Univ. Press) 278
McWilliam, A. 1990, ApJS, 74, 1075
Mermilliod, J.-C., & Mayor, M. 1992, in Binaries as Tracers of Stellar Formation, ed. A. Duquennoy, & M. Mayor (Cambridge: Cambridge Univ. Press) 183
Mermilliod, J.-C., & Nitschelm, C. 1989, A&AS, 81, 401
Nordström, B., et al. 2004, A&A, 418, 989
Ochsenbein, F., Bauer, P., & Marcout, J. 2000, A&AS, 143, 221
Parsons, S. B. 1983, ApJS, 53, 553
Parsons, S. B., & Ake, T. B. 1998, ApJS, 119, 83
Plummer, H. C. 1908, Lick Obs. Bull., 5, 24
Pourbaix, D. 2000, A&A, 145, 215P
Pourbaix, D., et al. 2004, A&A, 424, 727
Radford, G. A., & Griffin, R. F. 1975, Observatory, 95, 143
Ramirez, I., & Melendez, J. 2005, ApJ, 626, 465
Sandquist, E. L., Dokter, J. J., Lin, D. N. C., & Mardling, R. A. 2002, ApJ, 572, 1012
Sandquist, E. L., Taam, R. E., Lin, D. N. C., & Burkert, A. 1998, ApJ, 506, L65
Sanford, R. F., & Karr, E. 1942, ApJ, 96, 214
Setiawan, J., Pasquini, L., da Silva, L., Hatzes, A. P., von der Lühe, O., Girardi, L., de Medeiros, J. R., & Guenther, E. 2004, A&A, 421, 241
Snowden, M. S., & Young, A. 2005, ApJS, 157, 126
Scarfe, C. D., & Alers, S. 1975, PASP, 87, 285
Siess, L., & Livio, M. 1999a, MNRAS, 304, 925
Siess, L., & Livio, M. 1999b, MNRAS, 308, 1133
Skrutskie, M. F., et al. 2006, AJ, 131, 1163
Soker, N., Harpaz, A., & Livio, M. 1984, MNRAS, 210, 189
Spencer Jones, H. 1928, MNRAS, 88, 644
Strassmeier, K. G., Fekel, F. C., Gray, D. F., Hatzes, A. P., Schmitt, J. H. M. M., & Solanski, S. K. 1998, in ASP Conf. Ser. 154, The 10th Cambridge Workshop on Cool Stars, Stellar Systems and the Sun, ed. R. A. Donahue, & J. A. Bookbinder (San Francisco, CA: ASP) 257
Thompson, M. J., Christensen-Dalsgaard, J., Miesch, M. S., & Toomre, J. 2003, ARA&A, 41, 599
Tokovinin, A. A., Shatskii, N. J., & Magnitskii, A. K. 1998, Astron. Lett., 24, 795
Tokovinin, A. A., & Smekhov, M. G. 2002, A&A, 382, 118
Torres, G., Stefanik, R. P., & Latham, D. W. 1997, ApJ, 485, 167
Underhill, A. B. 1963, Publ. Dom. Astrophys. Obs., 12, 15
Valdes, F., Gupta, R., Rose, J. A., Singh, H. P., & Bell, D. J. 2004, ApJS, 152, 251
VandenBerg, D. A., & Clem, J. L. 2003, AJ, 126, 778
Vennes, S., Christian, D. J., & Thorstensen, J. R. 1998, ApJ, 502, 763
Walker, E. J. 1944, J. RAS. Can., 38, 249
Young, R. K. 1921, J. RAS. Can., 15, 161
Young, R. K. 1944, Commun. David Dunlap Obs., 12, 366
Zahn, J.-P. 1977, A&A, 57, 383
Zahn, J.-P. 1989, A&A, 220, 112
Zahn, J.-P. 1992, in Binaries as Tracers of Stellar Formation, ed. A. Duquennoy, & M. Mayor (Cambridge: Cambridge Univ. Press) 253
Zahn, J.-P., & Bouchet, L. 1989, A&A, 223, 112
Zucker, S., & Mazeh, T. 1994, ApJ, 420, 806